Experimental and theoretical study of the surface resonances on the (100) faces of W and Mo

Shang-Lin Weng,* E. W. Plummer, and T. Gustafsson

*Department of Physics and Laboratory for Research on the Structure of Matter, University of Pennsylvania,
Philadelphia, Pennsylvania 19104*

We present an experimental and theoretical study of the surface resonances on the (100) faces of W and Mo. From our experimental study, utilizing both angle-resolved photoemission with use of synchrotron radiation and angle-integrated photoemission, as well as field emission, we have documented the following properties of these surface resonances: (i) There are three occupied bands of surface resonances in the surface Brillouin zone. They are located about 0.2, 0.6, and 3.3 (0.3, 0.8, and 4.2) eV below the Fermi level for Mo (W). The dispersion is at most 0.3 eV for each band of surface resonances. (ii) The first band of resonances [at 0.2 (0.3) eV] is mainly d_{z^2} in orbital character. It forms the well-known "surface-state" peak in the field-emission spectra. (iii) The second band of resonances is primarily composed of $d_{x^2-y^2}$ and $d_{zx,zy}$ orbitals. It results in a shoulder below the "surface-state" peak in both the field-emission and angle-integrated photoemission spectra. Its photoemission intensity is zero at normal exit. (iv) The third band of resonances is similar to the first one and also made up of d_{z^2} and s orbitals. (v) As far as we can tell, many-body effects are not required to explain any aspect of the photoemission results from these resonances. The experimental data are compared to our calculation of the $\vec{k}_{\parallel}$- and orbital-resolved surface density of states, which uses a nonrelativistic tight-binding Green's-function scheme. The variations of the photoemission cross sections from these surface resonances are discussed in some detail and are shown to be determined by both macroscopic (i.e., the behavior of the electric field in the surface region, e.g., the reflection effects on the polarization vector) and microscopic (i.e., the details of the final-state band structure) effects.

I. INTRODUCTION

The past decade has witnessed a rapid growth of interest in the study of the electronic structure of transition-metal surfaces. This is due, in part, to their obvious technological importance, and in part, to the impetus provided by the availability of new experimental techniques. As a result of the rapid development of experimental techniques, an increasing supply of reliable data on clean, well-ordered single-crystal surfaces has been produced.[1] This, in turn, has spurred theoretical research in the development and application of models and computational techniques.[2,3] Notwithstanding this advance, theoretical progress on transition-metal surfaces has lagged behind that on semiconductor surfaces.[3] This is partly due to a comparative lack of experimental data which has attracted theorists to work rather on semiconductor surfaces, and partly to the complexity arising from the d electrons, which make realistic calculations for transition metals difficult.

From a physicist's point of view,[2,3] a complete study of the electronic structure of solid surfaces has to take into account the following three types of wave function, namely, the scattering states, the surface states, and the surface resonances. The scattering states are specified by the requirement that deep in the bulk they consist of a single propagating Bloch wave carrying current toward the surface, and one or more reflected Bloch waves. Their energies are in allowed bands. The surface states are composed, however, purely of decaying evanescent Bloch waves in the bulk, and thus are bound to the surface. They can exist for particular energies which lie in gaps or forbidden regions for a given $\vec{k}_{\parallel}$. The surface resonance, which involves scattering states, is closely related to the formation of a surface state. It generally occurs when a surface state is degenerate with bulk bands. In such cases, the state will decay into the bulk, since $k_{\perp}$ is not a good quantum number, and thus forms a resonance.

Surface states (surface resonances) are by their very nature one of the most specific features to the electronic structure of solid surface. These states (resonances) are fairly common and well understood on semiconductor surfaces,[3] but comparatively little is known about such features on metal surfaces. The most studied metallic surface resonances occurs on the (100) plane of tungsten.[4] This feature was first discovered by Swanson and Crouser[5] in a field-emission energy distribution (FEED) from W(100). Somewhat later, a very similar feature was observed on the electronically very similar (100) face of Mo.[6] The peak on W(100), which Swanson and Crouser[5] called "anomalous structure" and interpreted in terms of the relativistic bulk band structure, was shown to be very sensitive to contamination—and first identified as a surface state—by Plummer and Gadzuk[7] in a later FEED

study. A similar feature was also observed in a quite different type of experiment, photoemission,[8,9] showing that it was characteristic of the electronic structure of this metal surface. It is interesting that the three metallic surface states that were first discovered [W(100),[5] Mo(100),[6] and[10] Cu(111)] were all first observed with field emission energy distributions. It is also of some interest to note that they were all first interpreted[5,6,10] in terms of the bulk energy-band structure.

With the advent of angle-resolved photoelectron spectroscopy many additional characteristics of the surface resonances on W and Mo(100) have been reported. Several of these studies[11-14] have been concerned with the photoelectric excitation mechansim associated with these resonances as well as initial-state properties.[15-17] This, in turn, has introduced arguments about many-electron effects, like "time-dependent relaxation"[11] and "plasma interaction,"[12] and "d-band edge" effects[13] into the interpretation of this feature.

Several different theoretical studies concerning the origin of these resonances have been developed with the experimental progress. Roughly speaking, the evolution of the theory has generated five different types of interpretations which have attributed this "anomalous structure" to: (a) Bulk electronic structure. Two different such interpretations have been proposed, one based on the lack of electron states just below the Fermi level (E_F),[5,18] and another on enhanced emission from flat d bands, superimposed on much wider s bands.[19] (b) A surface state at $\vec{k}_\parallel = 0$ arising from the spin-orbit interaction.[7,20-22] This interpretation is similar to the theory of the semiconductor surface state[3] and related to basic principles of the metallic surface state as proposed by Forstmann and Pendry.[33] This interpretation which relies on relativistic effects was questioned by a recent nonrelativistic calculation by Nicolaou and Modinos[24] who instead interpreted this feature as being due to a (c) surface resonance. This may be thought of as a surface state located in some nonrelativistic hybridization gap at a general point of $\vec{k}_\parallel$. This sharp state will eventually become a resonance due to its interaction with the bulk states. This interpretation was first proposed in a FEED model calculation and has been supported by later nonrelativistic calculations.[25-28] (d) Kasowski[29] has attributed this feature to a surface state in a nonrelativistic hybridization gap at $\vec{k}_\parallel = 0$. This gap, which has $s - d_{z^2}$ symmetry, is located too far below E_F in an ideal crystal to account for the observed feature. However, its energy position is sensitive to the

spacing between layers and can be made to shift upwards by a surface contraction.[29] Kasowski's interpretation has been supported by symmetry arguments.[30] (e) Finally, very recently the first self-consistent pseudopotential calculation of the electronic structure of Mo(100) has been reported. This calculation[31] is very different from all earlier ones, in that it yields not only one but two occupied surface resonances with Δ_1 character at $\vec{k}_\parallel = 0$ in the $s - d_{z^2}$ hybridization gap.[32]

For the past few years, we have studied the surface resonances on the (100) faces of W and Mo in several different ways. Experimentally, we have used two methods to study these features: the first is photoemission, both angle integrated using conventional light sources[33] and angle resolved using synchrotron radiation,[34] the second is field emission.[28,35] Theoretically, we have developed a calculation[28,35] of the $\vec{k}_\parallel$ - and orbital-resolved surface density of states, which uses a nonrelativistic tight-binding Green's-function scheme.

The purpose of the present paper is to discuss in more detail some of our already published data on these surface resonances[28,33,34] and to present additional experimental findings about them. In particular, we wish to stress the wealth of information obtainable from a careful analysis of the polarization as well as photon-energy dependence of angular resolved photoemission data. We also want to discuss our theoretical calculation[28,35] in more detail and critically compare it to other theoretical work.

The assignment of a peak in an angle-resolved photoemission spectrum to a surface state (resonance) is by no means straightforward. Before we have made such an assignment a peak has to fulfill the following four criteria: (i) It is sensitive to contamination. (ii) Its energy position is independent of photon energy. (iii) It is consistent with angle-integrated photoemission data. (iv) It is possible to understand as a surface state (resonance) from a theoretical calculation.

The material is organized as follows. In Sec. II we will briefly describe the experimental procedures that we have used. In Sec. III we present and discuss all the experimental data for these surface resonances. Section IV focuses on our own theoretical work. We will first briefly outline the formalism used in our model calculation, and then give a detailed analysis of the calculated results. Section V consists of a detailed comparison of the various theoretical calculations, including our own, with experiment in an attempt to assess the current understanding of these surface resonances. In the final section, we will give a brief summary and some conclusions.

II. EXPERIMENTAL TECHNIQUES

A. Angle-resolved photoemission

All of our angle-resolved photon-energy and polarization-dependent photoemission results were obtained at the 240-MeV storage ring at the Synchrotron Radiation Center of the Physical Sciences Laboratory of the University of Wisconsin using a system described elsewhere.[36] The radiation from the storage ring is dispersed with a 1-m vertically mounted Seya-Namioka monochromator. The wavelength resolution of the monochromator is externally variable and was set to correspond (at roughly $\hbar\omega = 22$ eV) to the energy resolution of the energy analyzer. As the wavelength resolution was held constant, independent of wavelength, the energy resolution will decrease as the photon energy is increased. This will, as will be discussed below, result in an increased width of all features at higher photon energies.

The spectra were taken with a 180° spherical energy analyzer[36] using a constant-pass energy and incorporating a series of retarding and accelerating lenses. The analyzer has an acceptance of ±2.5° and is independently rotatable around two orthogonal axes. The highest total energy resolution was about 0.12 eV, which enabled us to resolve the two surface resonances which occur at off-normal exit on both metal surfaces. In many cases it was sufficient to work instead at lower-energy resolution (approximately 0.4 eV) which resulted in reduced data accumulation times. The samples can be independently rotated around two orthogonal axes. One rotation changes the angle of incidence in p polarization, the other rotates the crystal around its normal.

A lot of the data presented in this paper are in the form of peak intensities for a given surface resonance. These peak intensities, being proportional to the cross sections for the resonances, were measured over an estimated smooth background. The assumption that the background is smooth is a reasonable one in many cases, but by no means always. In particular, when the surface resonance overlaps a direct bulk transition in a certain photon-energy range, errors may be introduced. This is the case for the low-lying surface resonance on Mo(100) between $\hbar\omega = 21$ eV and $\hbar\omega = 28$ eV. The peak heights obtained were normalized relative to each other with respect to variations in light intensity with electron beam current and the wavelength dependence of the monochromator transmission.

B. Angle-integrated photoemission

The angle-integrated photoemission spectra of Mo(100) (Ref. 33) were measured using unpolarized 16.85 eV (Ne I) and 21.22 eV (He I) radiation at 40° angle of incidence. The photocurrent was collected using Varian 60° four-grid LEED optics. The retarding field was modulated at 3.5 kHz and 0.14 V (peak to peak), and the signal detected by conventional phase-sensitive electronics. Spectra were averaged by use of multiple sweeps and a multichannel analyzer. A mass spectrometer, and Auger system, and LEED optics within the experimental chamber allowed us to check the residual gases and the crystal cleanliness.

C. Field emission

Measurements of the field-emission energy distributions of Mo (Refs. 29, 35) were performed with a Simpson-Kuyatt type 135° spherical deflection energy analyzer together with a series of decelerating lenses.[37] The resolution was about 0.02 eV at reasonable field-emission voltages and current densities. A field-emission microscope was used to monitor the cleanliness of the sample. Upon application of a high voltage (usually around 2000 V) on the tip, field-emitted electrons from a selected clean surface would then pass through the probe hole and enter the energy analyzer. Data were then collected via an electron multiplier and a multichannel analyzer.

The data collected were in the form of energy distributions $j'(\epsilon)$. Due to the tunneling nature of the experiment they are roughly exponential in nature. In order to express the data in a more comprehensible way, we have divided them by calculated free-electron energy distributions $j'_0(\epsilon)$.[7] The final result, $j'(\epsilon)/j'_0(\epsilon)$, is the so-called enhancement factor, $R(\epsilon)$, which removes the exponential nature of the energy distributions and reveals any non-free-electron structure.

D. Sample preparation

The samples for photoemission were well-polished single crystals of dimensions approximately $6 \times 6 \times 1$ ($10 \times 6 \times 1$) mm of W(Mo). They were initially cleaned by standard procedures, i.e., oxygen treatment (~8 × 10⁻⁶ Torr) at elevated temperature (~800°C) and repeated thermal flashing. The molybdenum samples were in addition cleaned by argon ion bombardment. Before the accumulation of a spectrum, the W(Mo) samples were briefly heated to 3000 °C (2300 °C). A typical data acquisition time was 2 min at a base pressure of 2 × 10⁻¹⁰ Torr.

The field-emission tip was obtained from a

wire by etching with the so-called floating thin-layer-emitter technique.[38] It was cleaned *in situ* by repeated flashing.

III. EXPERIMENTAL RESULTS

A. Angle-resolved photoemission

Using the criteria described in Sec. I, we have observed, on both metal surfaces, two surface resonances (one high lying and one low lying) at normal exit ($\theta = 0°$), and three surface resonances (two high lying and one low lying) at exit angles greater than 2°. In the following, we will systematically present the results that have prompted this statement. We will first discuss the features in our spectra that directly relate to the ground-state properties of the system. We will then discuss those features that are manifestation of the way the experimental probe that we are using, namely photoelectron spectroscopy, is interacting with the system under study.

As mentioned in Sec. II, we have the experimental capability to independently vary four angular variables, two related to the incoming photon and two to the collected electron. The coordinate system that we will use is shown schematically in Fig. 1.

1. Initial-state properties

For normal emission (Fig. 2), we have observed one high-lying surface resonance located 0.3 (0.4) eV below E_F for Mo (W); and one low-lying resonance located 3.3 (4.2) eV below E_F for Mo (W). The high-lying resonance remains symmetric and narrow for all photon energies between 10 and 40 eV. The apparent peak width is increasing slightly with photon energy. This is most noticeable for the $\hbar\omega = 40$-eV spectrum for W(100) and can be accounted for by the decreased energy resolution of the monochromator at shorter wave lengths. The peak width obtained after correction for monochromator resolution [0.25 (0.4) eV for Mo (W)] is nearly identical with the width observed in a field-emission spectrum [0.2 eV for Mo (Ref. 28) and 0.35 eV for W (Ref. 7)] (Fig. 2). There is thus no discrepancy as far as the peak width is concerned between the normal photoemission and field-emission data. Also shown are some earlier angular resolved photoemission data by Feuerbacher and Willis[11] on W(100) and by Noguera *et al.*[13] on Mo(100). The shape of their spectra differs considerably from our results. The explanation for these differences will be given below.

It has been suggested by others[14,39] that the -4.2-eV peak on W(100) may be a surface state (resonance). The arguments were somewhat
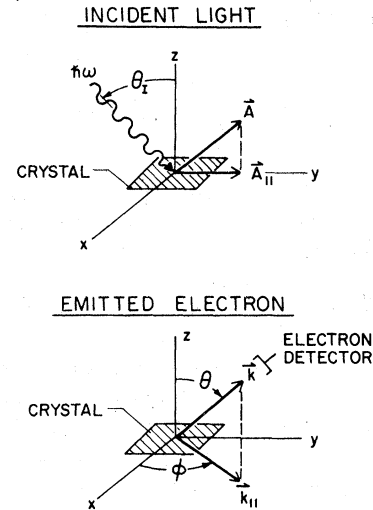
FIG. 1. Schematic drawings of the geometry of the angle-resolved photoemission measurements using synchrotron radiation.

speculative as they were mainly based on the fact that this peak is very sensitive to contamination. As stressed by us[34] and also by Noguera *et al.*[13] this is a necessary but not sufficient condition for its classification as a surface-state (resonance).
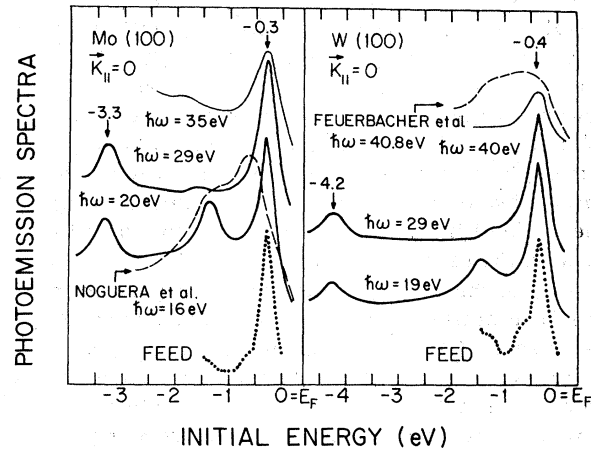
FIG. 2. Angle-resolved photoemission spectra of Mo(100) and W(100) at normal exit obtained with synchrotron radiation. The angle of incidence was 45° (*p* polarization). Dotted lines are the enhancement factors of the field-emission spectra of Mo(100) and W(100). The two peaks indicated by arrows are the high-lying and low-lying resonances. The photoemission data show additional structure, which moves in binding energy when the excitation energy is changed. We attribute this structure to direct transitions in the bulk. Dashed lines are some earlier photoemission data from Refs. 11 and 13.

HIGH LYING DOUBLET SURFACE RESONANCE
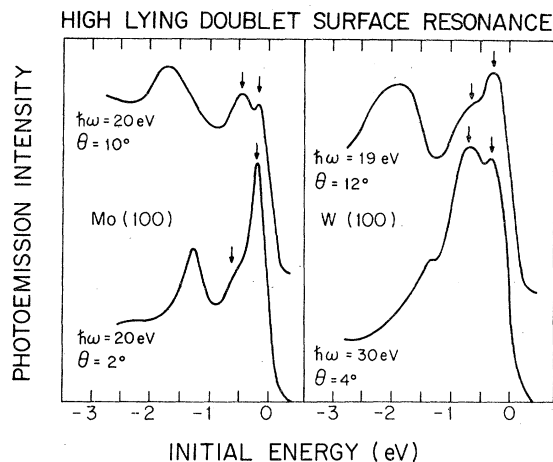
FIG. 3. Angle-resolved photoemission spectra of
Mo(100) and W(100) at various polar angles. The p-
polarized light was incident at 45°. θ is the collection
angle measured away from the surface normal. All
data refer to the plane perpendicular to the plane of
incidence. The two peaks indicated by the two arrows
are the two high-lying resonances.

For emission angles greater than 2° ($\theta > 2°$),
an additional second high-lying resonance appears
a few tenths of an eV below the first one. Figure
3 shows several photoemission spectra of both
metals at various polar angles and photon en-
ergies. For W, the data were taken in a (110)
mirror plane which is perpendicular to the plane
of incidence. For Mo, the data were taken in a
(100) mirror plane, which is also perpendicular
to the plane of incidence. As shall be discussed
in Sec. III A 2, the relative geometry between the
polarization vector $\vec{A}$ and the plane of emission
can influence the observed photoemission in-
tensity of the second resonance dramatically.
Although their intensities may vary, three distinct
surface resonances can be observed off normal
up to about 20° polar angle. For the sake of brev-
ity, we will refer to the resonance which is closest
to E_F as the first resonance; and to the low lying
one as the third resonance.

The energy splitting of the two high-lying res-
onances is about 0.35 (0.5) eV for Mo (W). We
wish to stress that the observation of the second
high-lying resonance is extremely sensitive to
the detection angle. We found that in order to
observe a single symmetric high-lying reso-
nance, the detector had to be aligned to with the
normal to within 1°. Even if the detector deviated
away from the normal with an angle as small as
2°, the second high-lying resonance will appear
as a shoulder in most directions (it may in a few
cases be suppressed due to the polarization ef-
fects discussed later). As the angle increases,
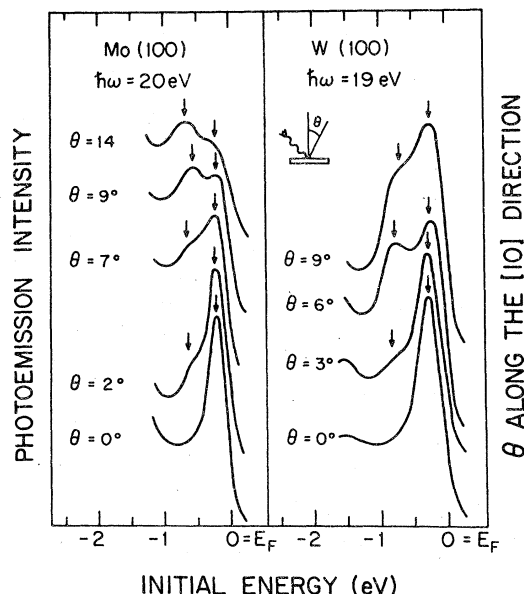
FIG. 4. Angle-resolved photoemission spectra of
Mo(100) and W(100) at various polar angles θ along the
[10] direction. The two high-lying surface resonances
are indicated by the two arrows. The second reson-
ance disappears at normal exit. The p-polarized light
was incident at 45°. All data refer to the plane per-
pendicular to the plane of incidence.

the second resonance increases its relative in-
tensity, while the first high-lying resonance in
general decreases its intensity. Figure 4 shows
these two high-lying resonances develop as a
function of the polar angle along the [10] direction
for fixed photon energy of both metal surfaces.
The data were taken in a (100) mirror plane which
is perpendicular to the plane of incidence. The
data indicate that the second resonance disappears
without merging into the first resonance as the
polar angle goes to 0°.

We show in the following figures the dispersion
and the intensity variation of these three surface
resonances along the [10] and the [11] directions
of both metal surfaces. Figure 5 shows the dis-
persion and the intensity variation of the two
high-lying resonances of W(100) as a function of
$k_{\parallel}$ along the [11] direction measured with two
photon energies (19 and 29 eV). The $\vec{k}_{\parallel}$ vector
is perpendicular to the plane of incidence. The
plot clearly shows that the intensity of the first
high-lying resonance peaks at normal exit and
decreases rapidly as $k_{\parallel}$ increases, in agreement
with a previous measurement.[15] The intensity
of the second high-lying resonance is completely
zero at normal exit but increases gradually with
increasing polar angle and reaches its maximum
value around $\theta = 10°$. As the polar angle keeps
increasing, the intensity decreases again. It is
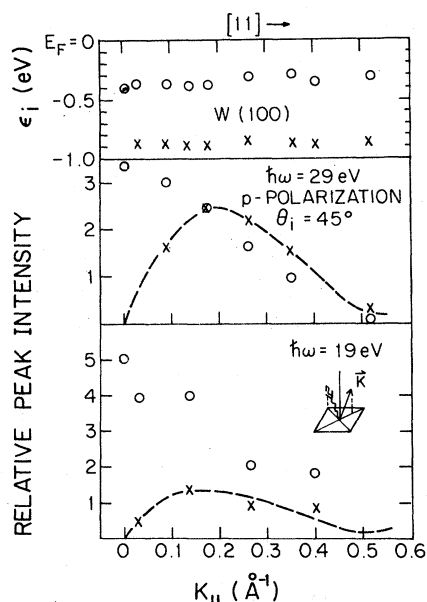
FIG. 5. Dispersion (top panel) and the photoemission intensity (bottom panel) of the first resonance (open circles) and the second resonance (✕) of W(100) plotted as function of $k_\parallel$ along the [11] direction. All data refer to the plane perpendicular to the plane of incidence. The dashed lines indicate the photoemission intensity of the second high-lying resonance as a function of $k_\parallel$.

interesting to note that the relative intensity of both resonances depends on the photon energy used. At the higher photon energy, the intensity of the second resonance is larger in relation to the first resonance for fixed $\vec{k}_\parallel$. These phenomena
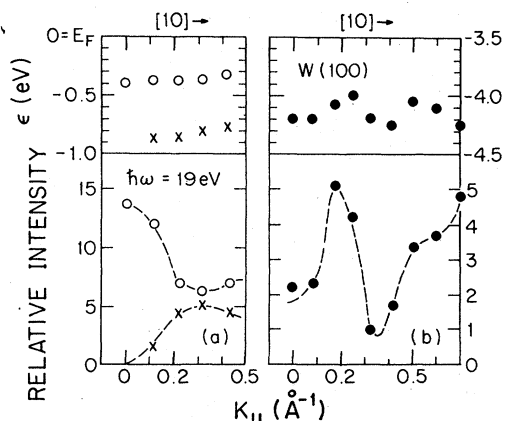
FIG. 6. Dispersion and the photoemission intensity of (a) the two high-lying resonances and (b) the low-lying resonance of W(100) plotted as function of $k_\parallel$ along the [10] direction. The dashed lines indicate the measured intensity variations of these resonances as function of $k_\parallel$.
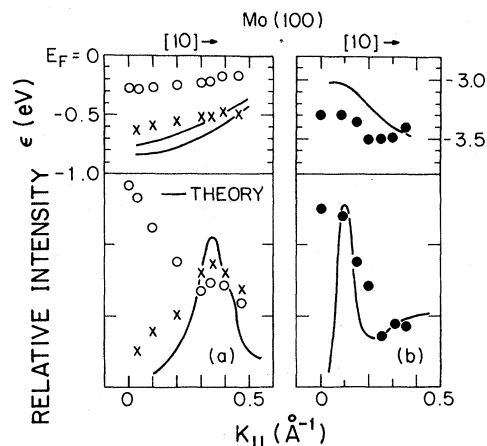
FIG. 7. Dispersion and the photoemission intensity of (a) the two high-lying resonances and (b) the low-lying resonance of Mo(100) plotted as function of $k_\parallel$ along the [10] direction. The photon energy is 30 eV. The solid curves are the calculated results which are discussed in Sec. IV.

indicate that these two resonances are different in character. Indeed, they possess different polarization properties which will be discussed in Sec. III A 2. Figure 6 shows the same kind of data along the [10] direction of W(100). The dispersion and the intensity variation of the low-lying resonance along this direction has also been plotted. The dispersion of these resonances is in general quite small.

The dispersion and the intensity variation of the three surface resonances of Mo(100) along the [10] direction is shown in Fig. 7. Again, the intensity of the second high-lying resonance is completely zero at normal exit but increases with $k_\parallel$ and reaches its maximum value around $k_\parallel = 0.3$ $\mathrm{\mathring{A}}^{-1}$. For $k_\parallel$ larger than 0.3 $\mathrm{\mathring{A}}^{-1}$, the second high-lying resonance is larger in intensity than the first one. The solid lines in Fig. 7 are the dispersion and the relative surface density-of-states variation of the three resonances as calculated in our theory. The calculation will be discussed in detail in Sec. IV. Here we just want to point out the agreement between the experimental and the theoretical results of the second and the third resonances. As for W, the dispersion is insignificant.

From Figs. 3 and 4 it is clear what would happen if one had used an electron energy analyzer with a larger angular acceptance than ours. Instead of the symmetric line shapes observed in Fig. 2, we would observe an asymmetric line, with the asymmetry caused by the second resonance. This asymmetry should become more pronounced as the photon energy is increased, i.e., as one
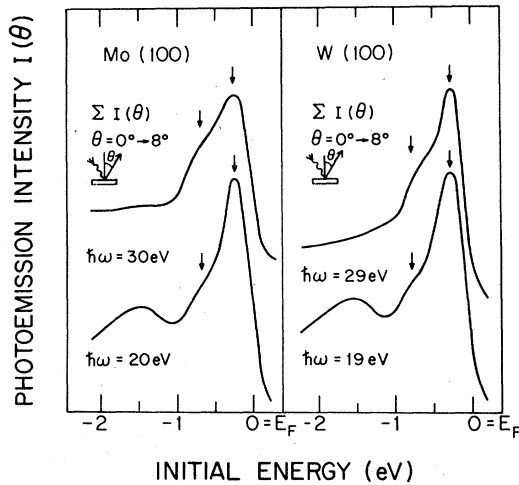
FIG. 8. Simulated angle-integrated photoemission spectra of W(100) and Mo(100) for a collection angle of ±8° around the surface normal. The spectra are average of our angle-resolved data (i.e., Figs. 4–6) over a cone of 8° half angle. The arrows indicate the two high-lying resonances.

integrates over larger $\vec{k}_{\parallel}$. To quantify this observation, we have averaged our data for $\hbar\omega = 19$ and 29 eV over a cone of half angle 8° (Fig. 8). The predicted asymmetry and its frequency dependence is observed. To reiterate, this is then what should be observed with an energy analyzer that has a larger angular acceptance than ours or one that is incorrectly aligned. A larger angular acceptance can arise, for example, if one has a large light spot and this defines the angular acceptance of the energy analyzer. The analyzer used in our work defines its own angular acceptance independent of the characteristics of the light spot.[36]

From Fig. 8 we can now reconcile the earlier $\vec{k}_{\parallel} = 0$ data[11,13] (see Fig. 2) with our findings. In particular we find that the linewidth of the first resonance on W(100) is *independent* of photon energy and it is hence not necessary to invoke time-dependent relaxation[11] to understand its shape. We also conclude that the first band of resonances on Mo(100) is located about 0.2 eV below E_F both in photoemission and field emission and not at 0.6 eV below E_F.[13]

The three surface resonances are found to be observable for $k_{\parallel} \leqslant 0.5$ Å^{-1} (Figs. 4–7), except at $\bar{\Gamma}(\vec{k}_{\parallel} = 0)$ where only two resonances are observed. The dispersion of these surface resonances is small, of the order of 0.3 eV. Consequently, these three bands of resonances are well separated. The two upper resonances tend to move towards E_F with $k_{\parallel}$, whereas the lowlying one tends to move away from E_F. This is true both for Mo and for W. No significant difference between different directions in the surface Brillouin zone is observed.

2. Photoemission properties

In addition to information about initial-state properties such as the resonance energies and the energy dispersion relation in the surface Brillouin zone (SBZ), their symmetry properties, and photon-energy dependence are also of interest and may yield additional information. Accordingly, we will in this subsection present our synchrotron photoemission results concerning (a) polarization effects, (b) the photon-energy dependence of the cross sections, and (c) the emission-angle dependence of the observed resonances.

a. *Polarization effects and symmetry.* Hermanson[30] has proposed a theoretical argument about the relationship between polarization effects and initial-state (final-state) symmetry properties. He has pointed out that, for emission normal to the surface or confined to a mirror plane containing the surface normal, the one-electron final state is invariant under crystal symmetry operations that leave the surface component of the momentum (i.e., $\vec{k}_{\parallel}$) unchanged. The symmetry of the initial state is then the same as that of the dipole operator causing the optical transition.

Following this argument, we immediately obtain the following symmetry selection rules for the initial states.

Rule I. For emission in a mirror plane, the one-electron final state has even parity (i.e., it possesses reflection symmetry with respect to the mirror plane). Accordingly, only those initial states which have the same parity as that of the dipole operator (or the polarization vector $\vec{A}$) will be excited.

Rule II. For emission in the normal direction, only Δ_1 and Δ_5 initial states can be excited on the (100) face of a *bcc* crystal. Moreover, the initial states with Δ_5 symmetry can only be excited by the surface component of the polarization vector, namely A_x or A_y. The initial states with Δ_1 symmetry can only be excited by the normal component, namely, A_z.

In Fig. 9 we show two angle-resolved photoemission spectra measured in a (110) mirror plane but with different polarization. For the upper spectrum, the $\vec{A}$ vector of the incoming p-polarized light is confined to the same (110) plane as the detected electron. Consequently, the dipole operator (or the $\vec{A}$ vector) has even parity with respect to this mirror plane. According to rule I, the initial states that can be excited must then have even parity. For the lower spectrum, the plane of the $\vec{A}$ vector is perpendicular to the plane

INITIAL ENERGY (eV)
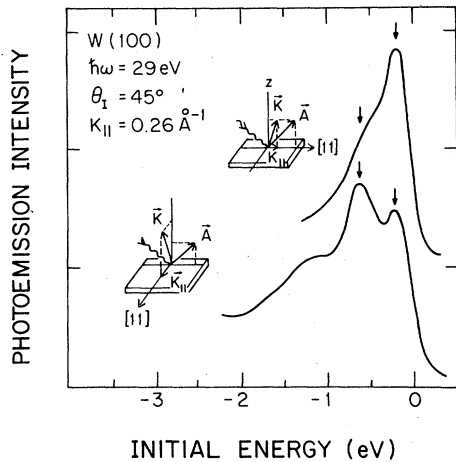
FIG. 9. Angle-resolved photoemission spectra of W(100) at $k_\parallel = 0.26$ Å^{-1} and $\hbar\omega = 29$ eV measured in a (110) mirror plane. The two peaks indicated by the two arrows are the two high-lying resonances. For the upper spectrum, the polarization vector $\vec{A}$ is in the same plane as the energy analyzer. For the lower spectrum, the $\vec{A}$ vector has been rotated by 90° around the surface normal. Hence the $\vec{A}$ vector has a component perpendicular to the mirror plane of collection.

of emission. Consequently, both even and odd parity of initial states can be excited, by A_z and $A_\parallel$, respectively. That is to say, the lower spectrum can contain intensity arising from initial states with odd parity which the upper spectrum can not. The data shown in Fig. 9 clearly indicate that the second high-lying resonance is much more pronounced in the lower spectrum than that in the upper spectrum. We therefore conclude that the second high-lying resonance possess odd parity with respect to the (100) mirror plane. Our calculation (see Sec. IV) is consistent with this experimental conclusion because the calculation shows that the second high-lying resonance is mainly made up of $d_{zx, zy}$ and $d_{x^2-y^2}$ orbitals for which the parity is odd with respect to the (110) mirror plane.

The fact that the second high-lying resonance appears weakly in the upper spectrum should indicate that this resonance also contains a small amount of even parity. However, this could also result from inaccuracies in alignment because the symmetry selection rules would be weakened if the $\vec{A}$ vector and/or the $\vec{k}_\parallel$ vector are not exactly in the mirror plane.

The polarization dependence of the first high-lying resonance (Fig. 9) obviously suggests that its parity is even because the upper spectrum can only contain initial states with even parity, e.g., d_{z^2} or s.

So far, we have concentrated on the orbital character of the double high-lying resonances

at $k_\parallel > 0$. We will now focus on the symmetry properties of the single high-lying resonance and the low-lying resonance at $\vec{k}_\parallel = 0$. According to rule II, the observable states at noramal exit must possess Δ_1 or Δ_5 symmetries. A state with Δ_1 symmetry can only be excited by the A_z component, while a state with Δ_5 symmetry can only be excited by the A_x component. One way to check the symmetry of the surface resonance would be to compare the photoemission intensity of this resonance in p and in s polarization. We have instead measured the angle of incidence dependence of these resonances for p polarization, which is in principle equivalent to the above mentioned test. The data for W(100) is shown in Fig. 10 and for Mo(100) in Fig. 11 (the high-lying resonance only). The measured intensities of both resonances are plotted on a relative scale. The calculated values of the two components of the $\vec{A}$ vector, namely, $|A_x|^2$ and $|A_z|^2$, are also plotted on a relative scale. The calculations of the field takes into account the macroscopic effects of reflection and refraction and uses classical electromagnetic formula.[40] The index of
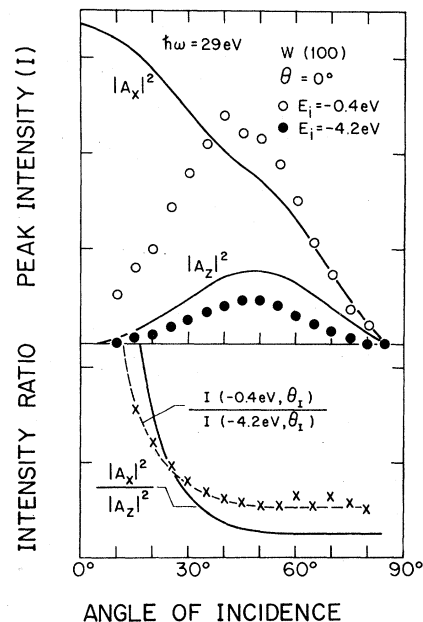
ANGLE OF INCIDENCE

FIG. 10. (Top) Photoemission intensity of the first (high-lying) resonance (open circles) and the third (low-lying) resonance (closed circles) at normal exit plotted as a function of the angle-of-incidence of the (p-polarized) light. The two solid curves are the calculated values of the two components of the polarized vector (see Fig. 1) on the surface of W. (Bottom) The ratio between the intensities of the two resonances (dashed curves) and also between the two components of the $\vec{A}$ vector (solid curves) obtained from the data shown in the top panel.
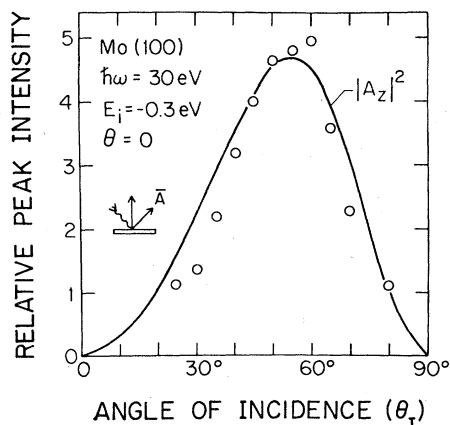
FIG. 11. Photoemission intensity of the first resonance of Mo(100) at normal exit plotted as a function of the angle of incidence of the (p-polarized) light. The photon energy is 30 eV. The solid curve is the calculated variation of $|A_z|^2$ with angle of incidence.

FIG. 12. Photoemission intensity of the first resonance of W(100) (circles) and Mo(100) (X) plotted as a function of the polar angle which has been converted into the surface momentum $k_{\parallel}$. The data are measured in the plane of incidence. The tungsten data are obtained at $\hbar\omega = 12$ eV (open circles) and $\hbar\omega = 29$ eV (filled circles), whereas the Mo data are for $\hbar\omega = 30$ eV.

refraction $\tilde{\eta} = n + ik$ are taken from the literature.[41,42] The data in Fig. 10 indicate that both resonances are excited by the A_z component. This suggests that the symmetry of both resonances is dominantly Δ_1. In other words, both resonances are mainly d_{z^2} and/or s in character.

However, the symmetry properties of the high-lying resonance at $\theta = 0°$ may possibly be complicated somewhat. In Fig. 10 we also show the ratio of the intensity from the –0.4-eV resonance to the –4.2-eV resonance as a function of angle of incidence. This is compared to the ratio of the light intensity parallel to the surface to the intensity perpendicular to it. We feel that such a comparison may be helpful to reveal second-order information about the symmetry properties. The fact that the ratio is not constant as a function of angle of incidence seems to suggest that the symmetry properties of both resonances are not quite the same. Specifically, since the intensity ratio of the high-lying resonance versus the low-lying resonance increases when the angle of incidence approaches 0° we may argue that the high-lying resonance is also excited by the A_x component. If this is the case, the high-lying resonance at $\theta = 0°$ must also contain some amount of Δ_5 symmetry, namely contain some amount of $d_{zx, zy}$-like orbitals. While it is tempting to attribute the observed trend to the inherent symmetry properties of the ground state, it may alternatively originate from the finite acceptance angle of the energy analyzer. The reason is as follows. At $\theta > 1°$, we know that the second high-lying resonance would appear. Consequently, a substantial amount of second high-lying resonances would be collected in the normal direction

because of the finite collection angle ($\pm 2.5°$). Since the second high-lying resonance is mainly $d_{zx, zy}$ and $d_{x^2-y^2}$ in character, the high-lying resonance measured in the normal direction would then weakly show this symmetry.

As for the symmetry properties of the high-lying surface resonance on Mo(100) at $\vec{k}_{\parallel} = 0$, a similar conclusion is obtained. As has been shown in Fig. 11, the data indicate that this high-lying resonance is excited by the A_z component of the polarization vector $\vec{A}$. According to rule II, we may conclude that this high-lying surface resonance possesses Δ_1 symmetry, namely, it has mainly d_{z^2}-like character.

  b. *Interference effects and polar-angle dependence.* In Fig. 12 we show the photoemission intensity of the high-lying resonance (s) as a function of the angle of collection (i.e., polar angle) for two different photon energies. We use p-polarized light and the plane of collection is chosen to be the plane of incidence, in this case a (110) mirror plane. The data shown in Fig. 12 were obtained with the electron-energy analyzer in the low-resolution mode (Sec. II). They are representative for the behavior of the first high-lying resonance as, for $\vec{k}_{\parallel}$ and $\vec{A}$ in the same (110) plane, the intensity from the second high-lying resonance is negligible (Fig. 9). The interesting observation in Fig. 12 is that the intensity at $\hbar\omega = 29$ eV is peaked off normal. More specifically, the intensity has here a maximum in the quadrant where $\vec{A}$ lies. Also there is a frequency dependence to the intensity distribution.

Data taken in a plane perpendicular to the plane of incidence is symmetric with respect to the

surface normal.

To explain these observations we will consider the symmetry properties of the photoexcitation cross-section matrix element for polarized light as oblique angles of incidence.

The photoemission cross section is proportional to the square of a matrix element

$$\sigma(\omega) \propto |\langle f|\vec{A}\cdot\vec{p}+\vec{p}\cdot\vec{A}|i\rangle|^2 .$$

It is clear from this expression that the value of the cross section depends upon three different quantities: the initial state $|i\rangle$, the final state $|f\rangle$, and the polarization vector $\vec{A}$.

For p-polarized light, the $\vec{A}$ vector can be resolved into two components, namely, $\vec{A}_{\parallel}$ and $\vec{A}_z$. Therefore, if we express the matrix element $\langle f|\vec{p}|i\rangle$ by a complex vector $\vec{M}=\vec{M}_{\parallel}+\vec{M}_z$

$$\sigma(\omega) \propto |A_{\parallel}M_{\parallel}+A_zM_z|^2$$

$$= |A_{\parallel}M_{\parallel}|^2 + |A_zM_z|^2 + 2\,\mathrm{Re}[(A_zM_z)^*A_{\parallel}M_{\parallel}] ,$$

where A_zM_z may contain the gradient part of the A_z component.

Let us confine our measurement to the (110) mirror plane in such a way that both the $\vec{A}$ vector and the detector lie in this plane. We fix the polar angle so that a state with a finite $\vec{k}_{\parallel}$ is probed. We then switch the location of the incident light beam from the quadrant spanned by the negative x asis and the z axis to the quadrant spanned by the positive x axis and the z axis, keeping the angle of incidence the same. The photoemission cross section will be changed by $4\,\mathrm{Re}[(A_zM_z)^* A_{\parallel}M_{\parallel}]$ because the value of $\vec{A}_{\parallel}$ will be changed from $+\vec{A}_{\parallel}$ to $-\vec{A}_{\parallel}$. This is equivalent to keeping the $\vec{A}$ vector fixed and moving the detector from $\vec{k}_{\parallel}$ to $-\vec{k}_{\parallel}$. That is to say, $M_{\parallel}$ will be changed from $+M_{\parallel}$ to $-M_{\parallel}$ when the surface momentum of the state, $\vec{k}_{\parallel}$, is changed from $+k_{\parallel}$ to $-k_{\parallel}$. This implies that the matrix element $M_{\parallel}$ must be an odd function of $k_{\parallel}$. Since this difference originates from the interference between the A_zM_z and $A_{\parallel}M_{\parallel}$ components of the matrix element, we call this asymmetric phenomenon an "interference effect." There are no obvious rules that determine the sign of this effect. This is due to the fact that it is a true interference effect and depends among other things on the relative phases of M_z and $M_{\parallel}$. Figure 12 does indeed suggest that the detected intensity for some materials and for some photon energies may be larger in the quadrant that does *not* contain the $\vec{A}$ vector.

We contend ourselves with the above qualitative discussion of the asymmetric shape of the intensity curve. A detailed theoretical calculation like the one for the Cu(111) surface state[43] is, of course, quite involved. It may be valuable,

however, because it might provide additional information about the initial-state properties of the first high-lying resonance.

By means of the data shown in Figs. 12 and 5, which were measured with different geometry of the polarization vector $\vec{A}$, we can in principle deduce the relative magnitude of the matrix element $|A_zM_z|^2$ and $|A_{\parallel}M_{\parallel}|^2$ as function of $k_{\parallel}$. The procedure is as follows.

First of all, if we add the intensity (Fig. 12) obtained for a particular $-\vec{k}_{\parallel}$ to the one obtained at $+\vec{k}_{\parallel}$ and divide by 2, the resultant intensity will be proportional to

$$f(k_{\parallel}) = |A_zM_z|^2 + |A_{\parallel}M_{\parallel}|^2 \quad (k_{\parallel} \geq 0)$$

because the interference terms will cancel out. (The above expression refers to the even-parity first high-lying resonance.)

Next, let us use the data in Fig. 5. These data were taken with the vector $\vec{A}$ in a plane perpendicular to the plane of emission [a (110) mirror plane]. In Sec. III A 2 a, we have shown that there is little odd-parity part associated with the first high-lying resonance. Consequently, the intensity curve of the first high-lying resonance is proportional to

$$g(k_{\parallel}) = |A_zM_z|^2 \quad (k_{\parallel} \geq 0) .$$

It is clear then that $g(k_{\parallel})$, namely, the data shown in Fig. 5 (the first high-lying resonance at $\hbar\omega = 29$ eV), gives the relative magnitude of $|A_zM_z|^2$ as a function of $k_{\parallel}$. The function $f(k_{\parallel})$ is also easy to obtain from the data shown in Fig. 12. If we substract $g(k_{\parallel})$ from $f(k_{\parallel})$, we obtain $|A_{\parallel}M_{\parallel}|^2$ as a function of $k_{\parallel}$.

The curves for $|A_zM_z|^2$ and $|A_{\parallel}M_{\parallel}|^2$ can be found elsewhere.[35] Schematically, $|A_zM_z|^2$ is the one shown in Fig. 5 and $|A_{\parallel}M_{\parallel}|^2$ looks like a Gaussian, centered around $k_{\parallel} = 0.25$ Å^{-1}, and approaching zero above $k_{\parallel} = 0.5$ Å^{-1} and below $k_{\parallel} = 0$. At its maximum, it is about as large as $|A_zM_z|^2$ at that $\vec{k}_{\parallel}$.

c. *Photon energy dependence.* The photoexcitation cross sections in photoemission depends on the initial state, the final state, and the polarization vector $\vec{A}$ as seen from the photoexcitation matrix element discussed in Sec. III A 2 b. Now, using the surface resonances of W(100) and Mo(100) as the initial states, we wish to demonstrate how the final-state band structure and the macroscopic polarization vector $\vec{A}$ affect the photoemission intensities of these surface resonances. Our approach is to sweep the photon energy, taking advantage of the continuous nature of synchrotron radiation. By sweeping the photon energy, we probe different final states and also change the polarization vector $\vec{A}$, which macroscopically de-

pends on the photon energy. This dependence is due to refraction[44] and reflection.

i. Microscopic effects: Final-state band structure. In Fig. 13 we show the photon-energy dependence of the photoexcitation cross sections for the two surface resonances at $\vec{k}_{\parallel} = 0$ both for W(100) and for Mo(100). One may first notice that the photoexcitation cross section from these resonances has a maximum at quite low photon energies. The signal from these resonances is maximized neither in absolute terms (Fig. 13) nor relative to the bulk emission when the probing depth has a minimum. The data for W(100) are in quite good agreement with the early data by Waclawski and Plummer,[8] especially if one considers the differences in collection geometry. Lapeyre *et al.*,[14] have also reported measurements of the transition strength from the high-lying resonances on W(100). The quantity that they evaluate is the ratio between the emission intensity at Fermi level for the clean and the adsorbate covered surface. It is *a priori* not clear how closely this quantity mimics the cross section. The agreement between their data and our (cross section) data (Fig. 13) is not good.

The cross sections in Fig. 13 exhibit final-state "resonance" effects which we to avoid confusion will call "photo resonances." For the high-lying
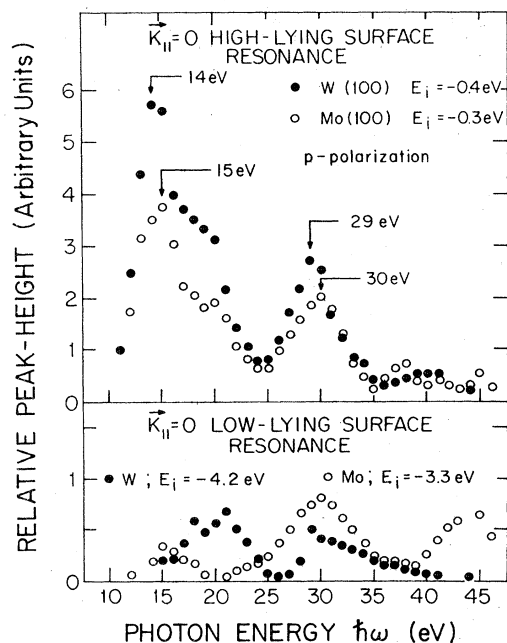
resonance, the photo resonances occur at $\hbar\omega = 15(14)$, $30(29)$ and 38 eV for Mo (W). In addition, a pronounced shoulder is observed at $\hbar\omega = 18$ eV for both metals. A lot of this structure is due to final state effects. To show this, we show a set of normal emission spectra in Fig. 14. The spectra are plotted as a function of the electron kinetic energy in vacuum, which by adding the work function [4.64 eV for W(100)] is easily converted into final-state energy above the Fermi level inside the crystal. It is clear from this figure that two pronounced peaks (indicated by the two dotted lines) appear in the secondary emission spectra at two kinetic energies $E_k = 10$ and 13 eV (or alternatively, at final state energies $E_F = 14.6$ and 17.6 eV). The higher final state at $E_k = 13$ eV (or $E_F = 17.6$ eV) is much broader (about 3-eV wide) than the lower one at $E_k = 10$ eV (about 1-eV wide). Remembering that $E_F = \hbar\omega + E_i$ in a one-electron scheme, we would expect that an enhanced photoexcitation cross section for the surface resonances may occur when $\hbar\omega + E_i$ is equal to either 14.6 or 17.6 eV. For the high-lying resonance ($E_i = -0.4$ eV) this leads us to expect enhanced photoexcitation cross section at $\hbar\omega = 15$ and 18 eV. Since the higher final state at $E_F = 17.6$ eV is much wider than the lower one, the enhanced cross section, or the photo resonance, at $\hbar\omega = 18$ eV would be *broader* than the one at $\hbar\omega = 15$ eV. This is exactly what is observed (Fig. 13). The same mechanism is also important in order to explain the photo resonance structure of the low-lying surface resonance. For the low-lying resonance of W(100), $E_i = -4.2$ eV, and "photo resonances" would therefore occur at $\hbar\omega = 18$ and 21 eV. This is consistent with our observation (see the lower part of Fig. 13).

It should in principle be possible to correlate the final state structure in Fig. 14 with experiments like secondary electron emission (SEE). Such comparisons are made more difficult by the "secondary cascade distribution cure" in the published SEE spectra.[45] We interpret this cascade to be due to the Auger decay of the $4f$ and $5p$ holes in tungsten. The photon energies used in Fig. 14 are below the threshold for excitations from these core levels and hence do not show any cascade effects.

Additional final state structure is seen in Fig. 14 for kinetic energies between 4 and 5 eV. This structure has been interpreted by Feuerbacher and Christensen[46] as being due to a band gap at the H point in the bulk Brillouin zone.

Egelhoff *et al.*[12] have argued that photoexcitation from the high-lying resonance on tungsten should become impossible at frequencies above the plasmon energy, which in tungsten is approximately

FIG. 13. Photoemission intensity of the high-lying and low-lying resonances on W(100) (closed circles) and Mo(100) (open circles) at normal exit plotted as a function of photon energy.
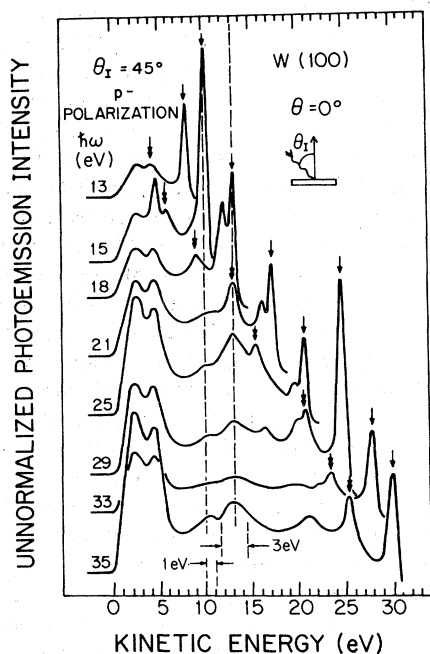
FIG. 14. Angle-resolved photoemission spectra of W(100) at normal exit measured with various photon energies. The spectra are plotted as a function of kinetic energy (i.e., final-state energy with zero of energy corresponding to the vacuum level). The high-lying resonance and the low-lying resonance are indicated by the arrow and the double arrow, respectively. Structure from two final states are seen in the secondary electron spectra and indicated by dashed vertical lines. The width of the lower final state is 1 eV, and of the higher one 3 eV.

25 eV. This suggestion was prompted by their inability to observe the resonance in a Ne II ($\hbar\omega = 26.9$ eV) spectrum. It was supported by an extremely simple model for the dielectric response of the metal. It is clear from Fig. 13 that, although the cross section for photoexcitation is fairly low at $\hbar\omega = 26$ eV, it is quite far from zero and increasing. We can understand the findings by Egelhoff et al.[12] by noting that they collected their spectrum 14° off the normal, where (Fig. 5) the cross section is quite low. The theoretical model they used may not be very helpful to describe tungsten, as the dielectric response is very far from free-electron-like[41] and the bulk plasmon is but poorly defined. We thus conclude that the high-lying surface resonance can be excited also above $\hbar\omega = 25$ eV,[11,14] and that there is no need to invoke many-electron phenomena (like plasmon coupling) to explain the photon energy dependence of the excitation from this resonance.

We thus conclude that microscopic effects, i.e., the final-state band structure, are important for an understanding of the photoexcitation cross

sections of these surface resonances. We will now turn to macroscopic effects.

ii. Macroscopic effects: reflection and refraction effects of $\vec{A}(\omega)$. We found above that the two surface resonances at $\vec{k}_\parallel = 0$ had d_{z^2}-like character and are mainly excited by the A_z component of the electric field. We also found above that the second high-lying surface resonance, which appears at $k_\parallel > 0$, had $d_{x^2-y^2}$ and $d_{zx,zy}$-like character and is mainly excited by the A_y component in a (110) mirror plane (A_y is perpendicular to this mirror plane). It is then reasonable to expect that major structure in $A_z(\omega)$ and $A_y(\omega)$ should show up in the cross sections of these surface resonances. Contrary to the final-state effects discussed above, which show up at fixed kinetic energies for both sets of resonances on the two metals, these effects should show up at fixed photon energies. From Maxwell's equations it follows that A_y but not A_z is continuous at the surface. The frequency dependence of A_z will also not be the same on both sides of interface. This provides a method to get some information about the spatial distribution of these surface resonances.

Let us focus on the polarization vector $\vec{A}(\omega)$ at the surface of tungsten as function of photon energy. The calculations are done for p-polarized light at 45° angle of incidence. The dielectric properties of the substrate are represented with a complex dielectric constant $\tilde{\epsilon}$ which is related to the index of refraction of the substrate $\tilde{\eta}$ by the following identity

$$\tilde{\epsilon} = \tilde{\eta}^2 .$$

The index of refraction $\tilde{\eta}$ is also assumed to be complex, namely, $\tilde{\eta} = n + ik$, with n and k taken, as before, from the literature.[41,42] The squared components of the polarization vector $\vec{A}$ are shown in Fig. 15. In the same figure we have also plotted the relative intensity of the high-lying and the low-lying resonances of W(100) observed at normal exit. Around $\hbar\omega = 25$ eV, $|A_z|^2$ (outside the surface) as well as the cross sections of both resonances possess minima. On the other hand, $|A_y|^2$ has a maximum. Such comparisons clearly indicate that both resonances are excited by the A_z component of the $\vec{A}$ vector and not by the A_y component. This is consistent with all the previous conclusions.

To reiterate: the important point is that the symmetry of the initial states such as the first high-lying resonance and the low-lying resonance allows a coupling to A_z. For initial states of different symmetry such as the second high-lying surface resonance no correlation with A_z is expected. Indeed, if we confine our measurement to a (110) mirror plane and let the plane of the

$\vec{A}$ vector be perpendicular to this mirror plane, then the major structure in $A_z(\omega)$ and $A_y(\omega)$ should show up in the cross sections of the first high-lying resonance and the second high-lying resonance, respectively, because the first (second) high-lying resonance is excited by the $A_z(A_y)$ component of the $\vec{A}$ vector (rule I).

In Fig. 16 we have plotted the relative intensity of the two high-lying resonances measured at $\theta = 12°$ in a (110) mirror plane. In the same figure we have also plotted the two components of the $\vec{A}(\omega)$ vector outside the surface [the plane of the $\vec{A}$ vector is perpendicular to the above mentioned (110) mirror plane]. Around $\hbar\omega = 25$ eV, $|A_z|^2$ as well as the cross section of the first high-lying resonance possess minima, whereas $|A_y|^2$ as well as the cross section of the second high-lying resonance possess maxima. Such comparisons clearly indicate that the first (second) high-lying resonance is excited by the A_z (A_y) component of the $\vec{A}$ vector. This is also consistent with all the previous conclusions.

It is sometimes argued in the literature that a useful criterion for a surface state (resonance) is that its excitation strength correlates with A_z. The theoretical justification for this "criterion" is very unclear. Our experimental data (Fig. 16) obviously directly refute it, showing that a surface state (resonance) depending on its symmetry may correlate with A_z or A_y.

In the following three figures, we will argue that the first high-lying surface resonances are excited by the A_z component just *outside* the surface. Figure 17 shows the photon-energy dependence of the components of the $\vec{A}$ vector on the surface of W (p-polarization at 45° angle of incidence). The photon-energy dependences of the two $|A_z|^2$ curves are apparently quite different. For A_z just outside the surface, $|A_z|^2$ has a minimum near $\hbar\omega = 25$ eV. For A_z just inside the surface, however, $|A_z|^2$ has a maximum around $\hbar\omega = 27$ eV and decreases rapidly (slowly) towards the low (high) photon energy side. Comparing with the data shown in Figs. 13 and 16, we find that the photon-energy dependences of the first high-lying resonance (and also the low-lying resonance) on W(100) correlate strongly with the A_z component just *outside* the surface, but does *not* correlate well with the A_z component just *inside* the surface. Moreover, we have also calculated[35] $|A_z \text{ (outside)} - A_z \text{ (inside)}|^2$ and found that this curve does not correlate well with the data either (this curve peaks at $\hbar\omega = 20$ eV and decreases rapidly towards the high-photon-energy side).

We therefore suggest that both resonances at $\vec{k}_\parallel = 0$ and the first high-lying resonance at $k_\parallel > 0$ mentioned above are excited by the A_z component
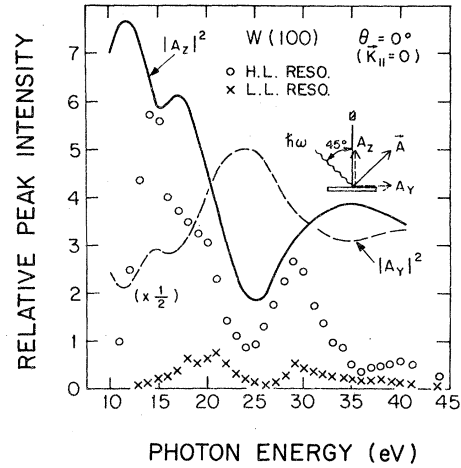
FIG. 15. Solid curve and dashed curve are the calculated values of $|A_z|^2$ and $|A_y|^2$ just outside the surface of W as function of photon energy for p-polarized light with 45° angle of incidence. The open circles and the crosses are the measured relative intensity of the high-lying and the low-lying resonances on W(100) at $\vec{k}_\parallel = 0$ as function of photon energy (Fig. 13).

just *outside* the surface. The same conclusion also holds for Mo(100). Figure 18 shows the components of the $\vec{A}$ vector just outside (upper panel) and inside (lower panel) the surface of Mo as function of photon energy. Also here, we find a close relationship between the data for the high-lying resonance (Fig. 13) and $|A_z|^2$ calculated just outside the surface. [The data for the low-lying resonance on Mo(100) is somewhat unreli-
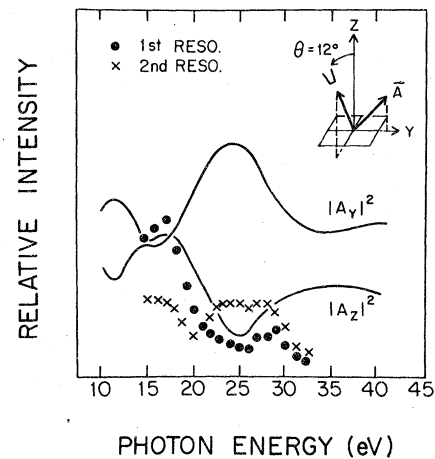
FIG. 16. Relative intensities of the two high-lying resonance measured at $\theta = 12°$ in a (110) mirror plane perpendicular to the plane of incidence (p polarization). The solid curves correspond to the calculated values of the electric fields parallel and perpendicular to (just outside) the surface for 45° angle of incidence.
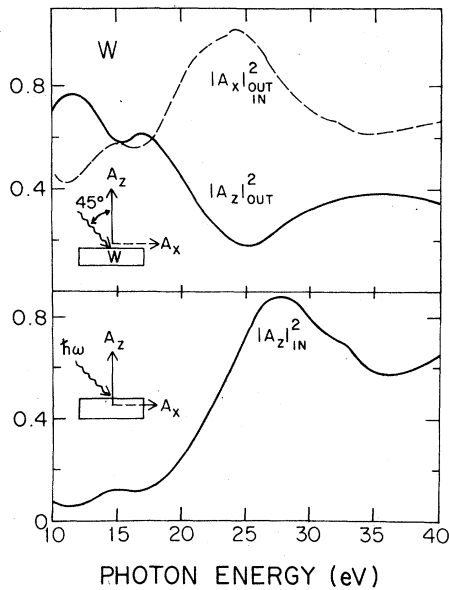
FIG. 17. Calculated values of (the square of) the electric field along and perpendicular to and just outside the surface (upper panel) and perpendicular to and just inside the surface (lower panel). The angle of incidence is taken to be 45° in p polarization and the optical constants of the metal are those appropriate to tungsten.
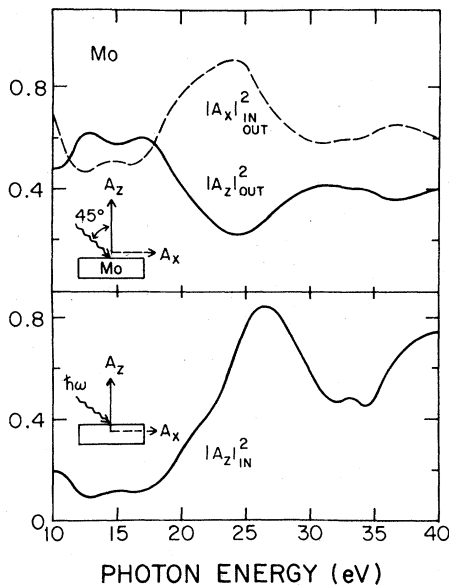
FIG. 18. Photon-energy dependence of (the square of) the electric field along and perpendicular to and just outside the surface (upper panel) and perpendicular to and just inside the surface (lower panel). The angle of incidence is taken to be 45° (p polarization) and the optical constants of the metal are those appropriate to molybdenum.

able due to interference from a direct transition, as mentioned above.]

The *photon-energy dependence* of A_z on *both* sides of the interface is evidently quite revealing. On the other hand there is *little* difference in the *angle of incidence dependence* of A_z outside and inside the surface for a fixed photon energy.[35] The main difference is a variation in the absolute magnitude of A_z between the two sides of the interface. Obviously (Figs. 17 and 18), the magnitude of A_z can increase or decrease when we cross the interface.

B. Angle-integrated photoemission

The angle-integrated photoemission data on Mo(100) have been presented elsewhere[33] and will for the sake of brevity not be discussed extensively here. They are in all aspects consistent with our angle-resolved photoemission data. Two sets of surface resonances were observed, both at $\hbar\omega = 21.22$ eV and at $\hbar\omega = 16.85$ eV. They are located 0.3 and 2.6 below the Fermi level. As the energy resolution is less good in the angle integrating apparatus the two high-lying surface resonances are not separately resolved. However, the angle-integrated data[33] provided the first experimental evidence for the prediction of a low-lying band of resonances on the (100) face of Mo.[28]

C. Field-emission energy distributions

Field-emission energy distributions (FEED) are obviously very surface sensitive. It is a very good tool to detect surface states (resonances), although in general the interpretation of FEED may be less than straightforward.[24,26] For tungsten, Plummer *et al.*[7,47] have shown that, among the four low-index planes [i.e., the (100), (110), (111), and (211) planes], only the (100) plane shows FEED structure that can be associated with occupied surface resonances. For molybdenum, a similar conclusion has been obtained by Weng.[28,35] In this section we will in particular attempt to show that the field-emission data are compatible with the photoemission data.

In Fig. 19 we show a comparison between the field emission and the photoemission spectra for both metal surfaces. The photoemission curves are the same as those shown in Fig. 8 and constructed from the angle-resolved photoemission data in such a way that they simulate the angle-integrated results for a collection angle of $\pm 8°$ around the surface normal. Such a summation is appropriate, as recent advances in the theory of field emission[24,26] suggest that this spectroscopy really measures electronic states over extended regions in $\vec{k}_\parallel$ space but with a heavy weight given
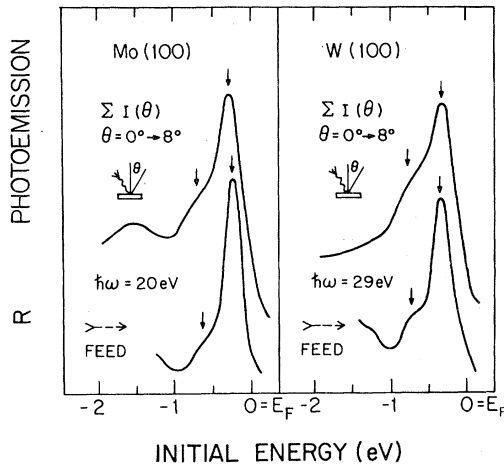
FIG. 19. Comparison between the resonance peak structure in the field-emission spectra and simulated angle-integrated photoemission spectra. The two curves in both panels are scaled in an arbitrary fashion relative to each other.

to states at $\vec{k}_{\parallel} = 0$.

The similarity between these two different sets of spectra is quite remarkable. For both metal surfaces, the well-known "surface-state" peak in the field-emission spectra is very similar to the main peak resulting from the first band of resonances in the photoemission spectra. The shoulder in the field-emission spectra is also similar to the shoulder in the photoemission curves, which originates from the second band of resonances. By means of this comparison, we thus reinterpret the field-emission spectra of the (100) faces of W and Mo as follows. (a) The well-known "surface-state" peak in the field-emission spectra originates from the first band of surface resonances. It is therefore d_{z^2}-like in character. (b) The shoulder below the "surface-state" peak originates from the second band of surface resonances. It is therefore $d_{x^2-y^2}$ and $d_{zx,zy}$-like in character. It is this shoulder, and not the "surface-state" peak, that existing field-emission theories[24,26] can explain.

It is not clear to what extent the different $\vec{k}_{\parallel}$ components of the first high-lying resonances contribute to the field-emission current. In particular, it is by no means obvious that the state of $\vec{k}_{\parallel} = 0$ is as important as a simple-minded comparison of the curves in Fig. 19 might lead one to conclude.

Another important feature which is related to the above conclusions and also provides a direct experimental evidence for the "$\vec{k}_{\parallel}$ integrated" nature of the field-emission current is the so-called "edge-proximity effect."[28] It occurs when the experiment probes electrons coming from an area near the (100) plane edge. Usually, when one probes electrons coming from the center of the (100) plane, the enhancement factor looks like the one shown in Fig. 19. A sharp resonance peak and a shoulder occur at -0.18 and -0.58 eV, respectively. However, when one probes electrons coming from near the plane edge, two significant phenomena occur: (i) the main resonance peak gets broadened; (ii) the energy positions of the main resonance and the shoulder shift away from the Fermi level by about a tenth of an eV (see Fig. 1 of Ref. 28).

The explanation for these effects[28] is as follows. We know that in the vicinity of the step edge the periodicity along the surface is destroyed. This would give rise to (a) a short mean-free path for the electron, and (b) the destruction of two-dimensional long-range order. The first effect leads to lifetime broadening, while the second prevents the component of $\vec{k}_{\parallel}$ (say, k_y) perpendicular to the edge from being a good quantum number for electron states near the edge. Both effects would result in a broadened peak as shown in Fig. 14 of Ref. 28.

Also, near the edge states of different k_y would mix, leading to a smearing out of the surface density of states. If the resonance peak in FEED were a consequence of a single resonance at one $\vec{k}_{\parallel}$ only, the effects discussed above would not result in a *shift* in the peak's energy position. Therefore, we conclude that there are contributions to the field-emission current from many different states at finite $\vec{k}_{\parallel}$. This is true for the well-known "surface-state" peak as well as the shoulder below.

The fact that the resonance peaks move in energy at the edge means also that the surface resonances possess *dispersive* characteristics.[28] Such dispersive characteristics can hardly be justified from our angle-resolved photoemission data (Figs. 5-7) because the photoemission energy resolution (about 0.12 eV) is much too low compared with the field-emission energy resolution (0.02 eV).[37]

Furthermore, the field dependence of the amplitude in the enhancement factor for Mo(100) (Refs. 28 and 35) independently shows that states at finite $\vec{k}_{\parallel}$ are involved. The situation for W(100) is less telling as far as the field dependence is concerned.

IV. THEORETICAL

In this section we will discuss in more detail the calculation[28,35] of the electronic structure of the (100) face of Mo. The purpose of this calculation is to provide independent support for many

of the arguments presented in the previous sections. Our primary interest in this paper is ground-state properties and not the physics of different spectroscopies. It is then appropriate that our calculation only addresses itself to the initial state. As shown in the previous sections it is by no means trivial to relate the measured spectra to such properties.

The theory that we are going to present[28,35] is a calculation of the $\vec{k}_{\parallel}$-and orbital-resolved surface density of states. It is based on the Slater-Koster interpolation scheme[48] (i.e., tight-binding scheme) and calculated using a Green's-function formalism similar to that used in bulk impurity problems.[2,49,50]

Our calculation differs in some aspects from earlier Green's-function calculations[25,50-52] of surface density of states. First, we have used nine types of atomic functions (s, p,and d) as the basis representation. The important sp-d hybridization effects are therefore included. Second, the tight-binding scheme used in this calculation has taken into account the hopping integrals up to the third nearest neighbors. The last and the most important distinction is that the surface density of states is obtained, as a function of energy, with respect to each orbital and each state of finite $\vec{k}_{\parallel}$ in the SBZ. We can therefore attempt to answer the following types of questions: (i) Where do the surface resonances exist in the SBZ? (ii) What is their dispersion? (iii) To what depth do they penetrate into the bulk? (iv) What kind of atomic-like orbitals do they consist of? and (v) Where are they located relative to the bulk band structure?

A. Formalism

Within the tight-binding scheme, we first construct the unperturbed Hamiltonian H_0 with use of nine atomic like orbitals (s, p, and d) as the basis representation. The matrix elements of H_0 are calculated using the formula shown in the paper by Slater and Koster.[48] We then proceed to construct the corresponding bulk Green's function P. The approach is similar to that used by Kalkstein and Soven[50] except that we have to consider nine atomic-orbital bases instead of one.

The calculation is done using a Wannier function or localized orbital basis. For simplicity we assume that the localized orbitals are mutually orthogonal. Furthermore, we assume that there are nine atomic orbitals associated with each atom.

We form the semi-infinite crystal by starting with a perfect crystal and passing an imaginary cleavage plane in some crystallographic direc-

tion. The cleavage plane itself is simply a mathematical device which isolates the left- and right-hand sides of the crystal.

The local density of states is most easily obtained by first calculating the Green's function for the cleaved crystal. Let H_0 and H be the Hamiltonians for the perfect and cleaved crystals, resepctively, and let P and G be the corresponding Green's functions. These operators satisfy equations of the form

$$(E - i\delta - H)G = 1 , \tag{1}$$

where E is the energy and δ a positive infinitesimal. G is given in terms of P and the perturbation $V = H - H_0$ by the Dyson's equation

$$G = P + PVG . \tag{2}$$

To calculate the matrix element of the Green's function and the Hamiltonian, we first introduce a mixed Bloch-Wannier representation, which takes into account the lattice translational symmetry parallel to the cleavage plane. In this representation, the basis function is defined as follows

$$|\vec{k}_{\parallel}, n, \alpha\rangle = \frac{1}{\sqrt{N_{\parallel}}} \sum_{\vec{R}_{\parallel}} |\vec{R}, \alpha\rangle \exp[i\vec{k}_{\parallel} \cdot (\vec{R}_{\parallel} + \vec{\tau}_n)] , \tag{3}$$

which is Bloch-like with respect to translations parallel to the surface plane, but is localized near the nth crystallographic plane. The surface plane is chosen as $n = 1$. $\vec{k}_{\parallel}$ is a wave vector parallel to the surface plane. $|\vec{R}, \alpha\rangle$ is the atomiclike orbital α located at site $\vec{R}$. The coordinate vector $\vec{R}$ of an arbitrary atom is given as follows.

Let $\vec{d}$ be the vector normal to the cleavage plane whose magnitude is the spacing between adjacent crystallographic planes parallel to the cleavage plane. The atomic sites in each parallel plane form a regular two-dimensional array. If we choose the origin of coordinates at some site on the right-hand surface, then any other atom at that surface has a coordinate vector $\vec{R}_{\parallel}$ which is parallel to the cleavage plane. The coordinate vector $\vec{R}$ of an arbitrary atom is then given by

$$\vec{R} = n\vec{d} + \vec{R}_{\parallel} + \vec{\tau}_n , \tag{4}$$

where $n = 0, 1, ...,$ or $n = -1, -2, ...,$ for atoms on the right- and left-hand sides, respectively, and $\vec{\tau}_n$ is that translational vector, parallel to the cleavage plane, which brings the atom in the nth plane in coincidence with those on the right-hand surface.

In Eq. (3) $N_{\parallel}$ is the number of atoms in the surface plane. It has been shown that all distinct functions of this type are obtained when $\vec{k}_{\parallel}$ as-

sumes all allowed values in the two-dimensional surface Brillouin zone (SBZ).[50]

In terms of the basis set shown in Eq. (3) the mathematical statement of the existence of lattice translational symmetry parallel to the cleavage plane is embodied in the relations

$$\langle m, \alpha, \vec{k}_{\parallel} | P | n, \beta, \vec{k}_{\parallel}' \rangle = \delta(\vec{k}_{\parallel} - \vec{k}_{\parallel}') P^{\alpha\beta}(m-n, \vec{k}_{\parallel}),$$

$$\langle m, \alpha, \vec{k}_{\parallel} | G | n, \beta, \vec{k}_{\parallel}' \rangle = \delta(\vec{k}_{\parallel} - \vec{k}_{\parallel}') G^{\alpha\beta}(m, n, \vec{k}_{\parallel}),$$

$$\langle m, \alpha, \vec{k}_{\parallel} | V | n, \beta, \vec{k}_{\parallel}' \rangle = \delta(\vec{k}_{\parallel} - \vec{k}_{\parallel}') V^{\alpha\beta}(m, n, \vec{k}_{\parallel}).$$

$$\tag{5}$$

G and V depend upon m and n separately, but, as indicated, P depends only upon the difference m-n since it is the Green's function for the perfect crystal.

The explicit form of $P^{\alpha\beta}(\vec{k}_{\parallel}, m$-$n)$ can be obtained by calculating the following matrix element:

$$\langle \vec{k}_{\parallel}, m, \alpha | P | \vec{k}_{\parallel}', n, \beta \rangle$$

$$= \sum_{\vec{q}} \sum_{\vec{q}'} \sum_{i} \sum_{j} \langle \vec{k}_{\parallel}, m, \alpha | \vec{q}, i \rangle \langle \vec{q}, i | P | \vec{q}', j \rangle$$

$$\times \langle \vec{q}', j | \vec{k}_{\parallel}', n, \beta \rangle, \tag{6}$$

where $|\vec{q}, j\rangle$ is the eigenfunction of the unperturbed Hamiltonian H_0 and is a Bloch-type function, namely,

$$|\vec{q}, j\rangle = \frac{1}{\sqrt{N}} \sum_{\alpha} \sum_{\vec{R}} e^{i\vec{R} \cdot \vec{q}} C_{\alpha}^{j} |\vec{R}, \alpha\rangle. \tag{7}$$

From Eqs. (3), (6), and (7) we can obtain

$$P^{\alpha\beta}(\vec{k}_{\parallel}, E, m-n)$$

$$\equiv P_{mn}^{\alpha\beta}(\vec{k}_{\parallel}, E)$$

$$= \frac{1}{\pi} \sum_{i} \int_{-\pi}^{\pi} dk_{\perp} \frac{C_{\beta i}^{*}(\vec{k}) C_{\alpha i}(\vec{k}) e^{i(m-n)k_{\perp}d}}{E - \epsilon_{i}(\vec{k}_{\parallel}, \vec{k}_{\perp}) + i\eta}, \tag{8}$$

where $\epsilon_i(\vec{k})$ is the eigenvalue of H_0, and i is the band index.

Next the surface is introduced as a perturbation in the form of repulsive potentials V on two particular planes, which are labeled by $n = 0$ and $n = -1$. Furthermore, we assume that

$$V = V_0 \delta_{00} + V_{-1} \delta_{-1-1},$$

and

$$V_0 \rightarrow \infty,$$

$$V_{-1} \rightarrow \infty. \tag{9}$$

The projected local density of states for a given $\vec{k}_{\parallel}$ and E is given by

$$\rho_n^{\alpha}(\vec{k}_{\parallel}, E) = -\frac{1}{\pi} \operatorname{Im} G_{nn}^{\alpha\alpha}(\vec{k}_{\parallel}, E). \tag{10}$$

The total density of states per atom for a semi-

infinite crystal is

$$\rho(E) = -\frac{1}{\pi N} \sum_{\alpha} \sum_{n} \sum_{\vec{k}_{\parallel}} \rho_n^{\alpha}(\vec{k}_{\parallel}, E). \tag{11}$$

All the important information of the electronic properties associated with each plane n is contained in the Eq. (11). It gives the local density-of-states, for a given $\vec{k}_{\parallel}$ and E, contributed to by the atomic orbital α. It thus gives the $\vec{k}_{\parallel}$ and orbital-resolved local (at plane n) density of states at an initial energy E.

In particular, the $\vec{k}_{\parallel}$ and orbital-resolved surface density of states, which is of main interest, takes the form

$$\rho_s^{\alpha}(\vec{k}_{\parallel}, E) = -\frac{1}{\pi N} \operatorname{Im} G_{11}^{\alpha\alpha}(\vec{k}_{\parallel}, E). \tag{12}$$

From Eqs. (9) and (2), it is trivial to solve for the matrix element $G_{11}^{\alpha\alpha}$. From Eqn. (12), we then obtain a $\vec{k}_{\parallel}$ and orbital-resolved surface density-of-states as a function of energy.

B. Numerical results

For the (100) face of a bcc crystal, the surface Brillouin zone is a square with a side length of $2\pi/l$, where l is the length of the cubic side and is equal to 5.94783 a.u. for molybdenum.[53] The triangle shown in Fig. 20 is the first eighth of the SBZ.

We have obtained numerical results for the $\vec{k}_{\parallel}$ and orbital-resolved surface local density of states (SLDS) and bulk density of states (BDOS) of Mo(100).[28] The Slater-Koster interpolation parameters were taken from the work by Iverson and Hodges.[54] Because of numerical problems, we can not obtain information about δ-shaped true surface states but only about the wider surface resonances.

By summing over $\vec{k}_{\parallel}$, we obtain the total SLDS and total BDOS as function of energy (Fig. 21). While the results should be directly applicable to
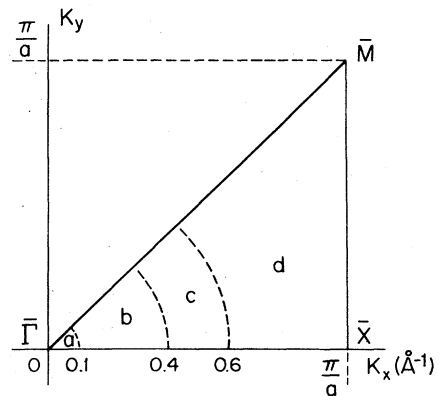
FIG. 20. Irreducible part of the surface Brillouin zone of the (100) face of bcc crystals.
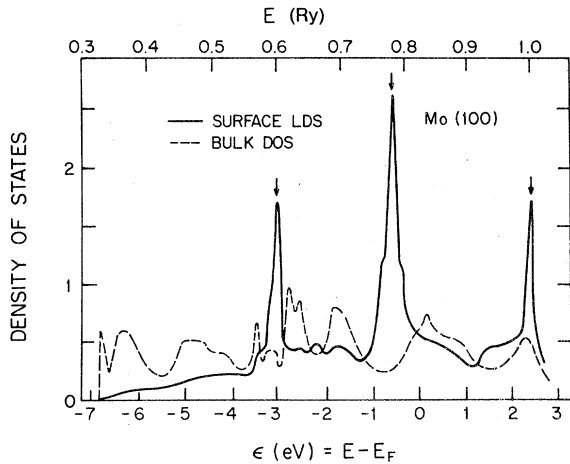
FIG. 21. Calculated total SLDS and total bulk DOS of Mo(100). Three bands of predicted surface resonances are indicated by arrows. The density of states is in arbitrary units.

Mo, the general shape of the curves should be representative for the bcc group-VIB transition metals, at least as long as relativistic effects are not important.

Our calculation suggests that the (100) face of these metals (W, Mo, and Cr) exhibits three major bands of surface resonances. Two of them are located below E_f. On the (110) face, however, we do not find any such structure using the same calculational scheme.[35]

1. High-lying occupied double surface resonances

Just below E_F, there is a band of pronounced surface resonances. This corresponds to the second band of high-lying resonances discussed above. According to this calculation, these high-lying resonances possess the following characteristics:

(a) These resonances are restricted to finite parallel momentum ($\vec{k}_{\parallel}$) between 0.1 and 0.6 Å⁻¹. Our angle-resolved photoemission data confirm this prediction.

(b) For a particular $\vec{k}_{\parallel}$ there exists two resonances quite close in energy. Their relative weight changes with $\vec{k}_{\parallel}$. The splitting in energy of these two high-lying resonances is about 0.14 eV (Fig. 22). For the example in Fig. 22 ($k_x = 0.2884$ Å⁻¹, $k_y = 0.0111$ Å⁻¹), the SLDS is extremely large for the state at $\epsilon = -0.65$ eV and is moderately large for the state at $\epsilon = -0.79$ eV. There two bands of resonances are so close that they are not resolved in experiment (cf. Fig. 7).

(c) The resonances display dispersive charac-teristics (Fig. 23). For $k_{\parallel}$ less than 0.6 Å⁻¹, the energy increases toward E_F as $k_{\parallel}$ increases along

	BULK DOS	SURFACE LDS
S	0	546.
P_X	0	12
P_Y	1.4	1.1
P_Z	0	6.7
d_{XY}	14.0	16.0
d_{YZ}	20.0	80.0
d_{ZX}	0.1	17490.
$d_{X^2-Y^2}$	0	11327.
$d_{3Z^2-r^2}$	0	199.
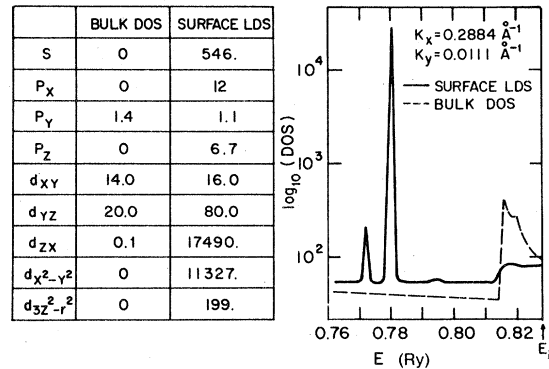
FIG. 22. Example of calculated SLDS for a particular $\vec{k}_{\parallel}$ in the high-lying occupied band of surface reson-ances. The table on the left-hand side shows the contri-bution from each orbital (in arbitrary units) of the SLDS of this resonance and to the bulk DOS at the same $\vec{k}_{\parallel}$.

the [10] direction (i.e., $\overline{\Gamma}\overline{X}$ in Fig. 20) or the [11] direction (i.e., $\overline{\Gamma}\overline{M}$ in Fig. 20). Along nonsymme-try lines, a more complex behavior is observed (Fig. 24).

(d) Most of the charge density associated with these resonances is confined to a small region of the SBZ (i.e., close to the $\overline{\Gamma}\overline{X}$ axis) of regions b and c in Fig. 20. Specifically, they are localized in the vicinity of a momentum: $k_x = 0.333$ Å⁻¹ and $k_y = 0.022$ Å⁻¹. To demonstrate this result, we show in Fig. 23 the SLDS of these resonances and their dispersion along the $\overline{\Gamma}\overline{X}$ direction for $k_{\parallel}$ < 0.5 Å⁻¹. Note that the resonances with momenta near $k_x = 0.3$ Å⁻¹ have the larger SLDS.

(e) These resonances are made up of d_{zx} (~ 60%), $d_{x^2-y^2}$ (~ 40%), and s (~ 2%) orbitals. An example has been shown in Fig. 22.
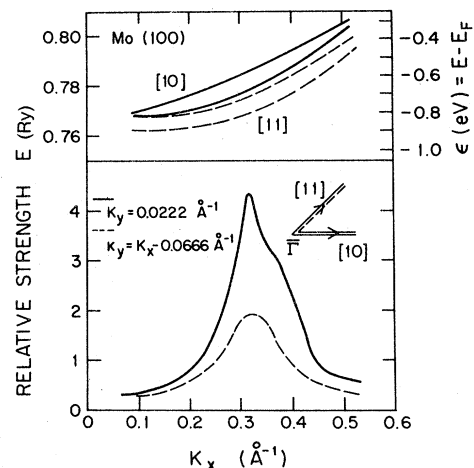
FIG. 23. Calculated dispersion and relative SLDS variation of the high-lying resonances along two direc-tions in the SBZ. These directions are very close to the [10] and [11] directions, respectively.
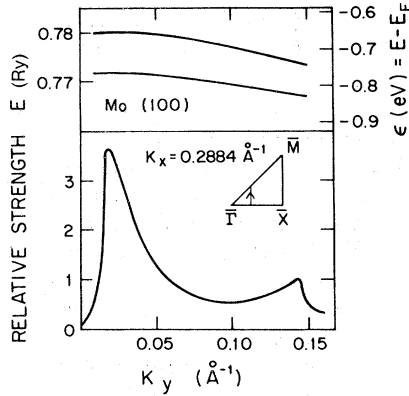
FIG. 24. Calculated dispersion along a nonsymmetry direction of the (doublet) high-lying resonance (upper panel). Also shown is the relative SLDS variation along the same direction (lower panel).

(f) To show the origin of these resonances, we first calculate the tight-binding bulk band structure at a state of finite $\vec{k}_\parallel$ ($k_x = 0.2884$ Å^{-1}, $k_y = 0.0111$ Å^{-1}) and at $\vec{k}_\parallel = 0$ (Fig. 25). The double high-lying resonances are indicated by a pair of dashed lines in Fig. 25(b). By comparing this band structure and the corresponding SLDS's and BDOS's we reach the following conclusion about their origin: they are located inside a hybridization gap [in Fig. 25(b), this gap spans from 0.73 to 0.81 Ry] which, when traced back to the band structure at $\vec{k}_\parallel = 0$ [Fig. 25(a)], is found to be related to the crossover of Δ_2 and Δ_5 bands. In other words, this hybridization gap, which occurs at a general point in the SBZ and does *not* occur at the $\bar\Gamma$ point, arises from two bulk bands which are mainly made up of d_{zx} and $d_{x^2-y^2}$ orbitals. Just like the
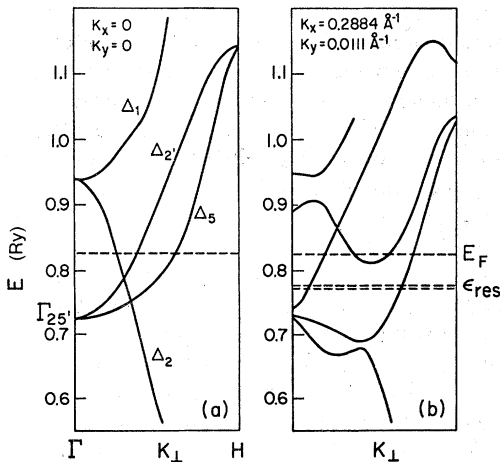
FIG. 25. (a) Calculated bulk band structure of Mo(100) at $\vec{k}_\parallel = 0$. (b) Calculated bulk band structure of Mo(100) at a finite $\vec{k}_\parallel$. The resonances are shown with dashed lines and located just below the Fermi level.
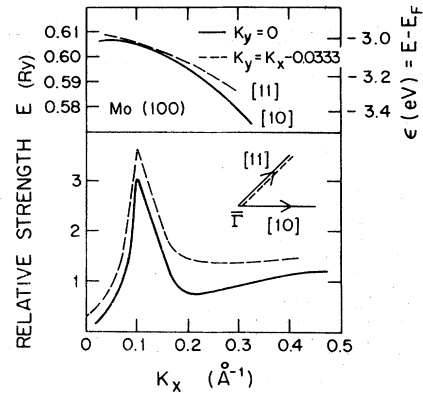
FIG. 26. Calculated dispersion and relative variation of the low-lying resonances along the [10] direction and the [11] direction.

creation of a surface state in a semiconductor bulk band gap,[3] a surface state is created in this metal nonsymmetric hybridization gap. It becomes a resonance because of its interaction with the other bulk states.

2. Low-lying occupied surface resonance

There is another band of surface resonances located at 3.02 eV below E_F on Mo(100). The prediction of this low-lying resonance is one of the most significant results in this calculation. It has been confirmed both in our angle-integrated[33] as well as angle-resolved[34] photoemission studied. As far as we know, it is the first time that a surface resonance on a metal surface has been predicted before it is observed experimentally.

(i) Its momentum is distributed in two main regions, one with $k_\parallel$ between 0 and 0.4 Å^{-1}, and the other with $k_\parallel$ between 0.7 and 0.9 Å^{-1}. The largest charge density is confined to the range 0.1 Å^{-1} $< k_\parallel < 0.3$ Å^{-1} (i.e., region b of Fig. 20). To demonstrate this result, we show in Fig. 26 the relative SLDS of these resonances as a function of $k_\parallel$. The dispersion (Fig. 26) is different from that of the high-lying resonances.

(ii) It is mainly composed of d_{z^2} ($\sim 75\%$), s ($\sim 14\%$), and p_z ($\sim 7\%$) orbitals (Fig. 27).

3. Unoccupied surface resonance

There is also a third band of resonances located 2.3 eV above E_F on Mo(100). They exist mainly in the region far away from the center of the SBZ (region d of Fig. 20). The orbital-resolved SLDS of one of these unoccupied resonances is shown in Fig. 28. They are made up of d_{z^2} and $d_{x^2-y^2}$ orbitals.

Empty surface resonances on W(100) have been shown, in an analysis of the secondary photoemis-

	BULK DOS	SURFACE LDS
s	0	269.5
p_x	0	4.4
p_y	0	4.0
p_z	0	164.5
d_{xy}	0	0.5
d_{yz}	0.3	7.6
d_{zx}	0.4	7.8
$d_{x^2-y^2}$	11.6	34.3
d_{z^2}	0	1446.4

$K_x = 0.1331$ Å^{-1}
$K_y = 0.0998$ Å^{-1}

— SURFACE LDS
--- BULK DOS
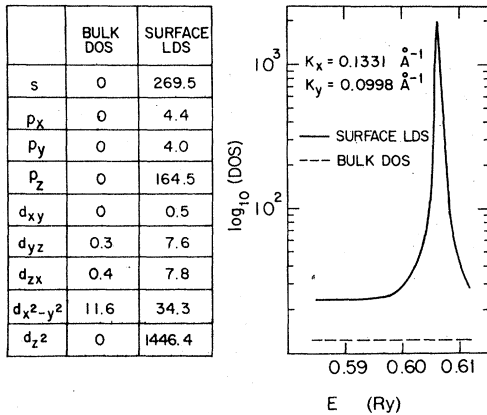
FIG. 27. Calculated SLDS of the low-lying resonance. The table on the left-hand side shows the contribution from each orbital to the SLDS (in arbitrary units) of this resonance and to the bulk DOS at the same $\vec{k}_\parallel$.

sion spectra of W(100),[55] to exist for $k_\parallel > 0.3$ Å^{-1} (up to the edge of the SBZ). This is consistent with our calculation.

V. DISCUSSION OF THE DIFFERENT THEORETICAL APPROACHES

As discussed in the introduction, several different theoretical calculations have been advanced in order to explain the surface states (resonances) on Mo and W. In this section we will try to compare these calculations.

We have so far implicitly assumed that the geometry of the crystal is unchanged at the surface and in particular that the spacing between the

	BULK DOS	SURFACE LDS
s	0	31.6
p_x	0	16.9
p_y	0.6	0.5
p_z	0.1	6.5
d_{xy}	6.4	6.7
d_{yz}	16.0	24.2
d_{zx}	1.2	235.9
$d_{x^2-y^2}$	0.4	1876.1
$d_{3z^2-r^2}$	0.1	4898.8

$K_x = 0.8986$ Å^{-1}
$K_y = 0.0998$ Å^{-1}
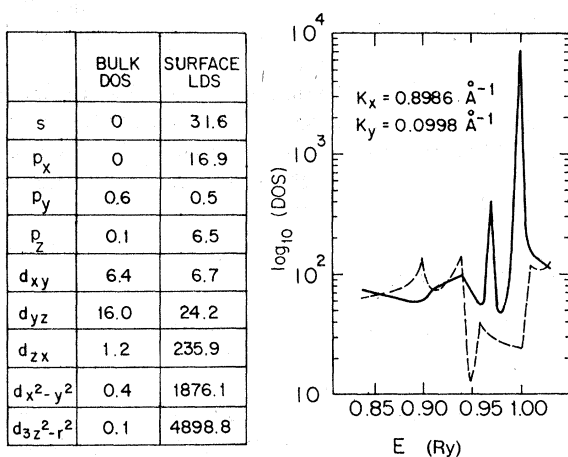
FIG. 28. Calculated SLDS of the unoccupied surface resonance. The table on the left-hand side shows the contribution from each orbital to the SLDS (in arbitrary units) of this resonance and to the bulk DOS at the same $\vec{k}_\parallel$.

outermost two atomic layers is the same as the bulk spacing. This assumption clearly needs to be justified.[13,29] Such justification is provided by two different experiments, both (more or less) direct probes of surface geometry. From an ion-scattering experiment, Feldman et al.[56] conclude that the layer spacing is at most 6% smaller than the bulk value. From an analysis of LEED data Debe et al.[57] suggest that this spacing is 4% smaller than in the bulk. (This value supercedes earlier LEED results.[58,59]) Any vertical displacements are thus quite small. Hence, there is little support for the mechanisms used by Kasowski[29] and by Noguera et al.[13] In the calculation by Kasowski[29] a d_{z^2}-s type surface state appears near the Fermi level for a contracted surface. This is the same state that we predict in our calculation for the unreconstructed surface at -3 eV and that we identify with the low-lying surface resonance in our spectra. This identification is, as we have seen above, supported by symmetry arguments. There thus seems to be little justification for invoking a surface contraction to explain the surface state (resonance) at the Fermi level.

One may then turn to the interpretations based on relativistic effects to explain the resonance of Δ_1 symmetry close to E_F at $\vec{k}_\parallel = 0$. However, as already shown by Hermanson,[30] the symmetry of the two surface states (both are Δ_7, that is Δ_2 and Δ_5 nonrelativistically) predicted in the relativistic calculation[21] are not the right ones. The relativistic calculation is also unable to explain the second high-lying resonance, as this resonance either does not exist at all or purely possesses Δ_2 symmetry at $\vec{k}_\parallel = 0$ (so that, according to rule II of Sec. III, it will not be excited at normal exit), in contradiction to predictions (Δ_2 and Δ_5).[21]

The nonrelativistic calculations for an unreconstructed surface yield results[24-28] in better agreement with experiments. They predict correctly the existence and symmetry of the low-lying resonance as well as the existence and orbital character of the second high-lying resonance. However, they are all unable to explain the first high-lying resonance.

The calculation[28,35] presented in Sec. IV has some additional assets that deserve mention. Without adjusting any parameters we obtain a separation between the high-lying and low-lying resonances in excellent agreement with experiment (see Ref. 33). Also the predicted dispersion agrees well with the experimental findings (see Fig. 7). However, it is now clear that it can *not* explain the *first band* of high-lying resonances, contrary to what was once claimed.[34] Our polarization studies clearly show that the symmetry of the first band of high-lying resonances is not

compatible with the symmetry of the first high-lying resonance calculated (Fig. 22). Also the splitting in energy is calculated to be too small. *To reiterate*: all *non-self-consistent* calculations of the surface electronic structure are *unable* to predict the existence of the first band of high-lying surface resonances on W(100) and Mo(100).

Very recently, Kerker *et al.*[32] have self-consistently calculated the surface electronic structure of Mo(100) using a pseudopotential formalism. At $\vec{k}_{\parallel} = 0$, this calculation yields not one, but two occupied surface resonances with Δ_1 symmetry. Although some problems do exist (especially for the orbital character of the two high-lying resonances at $k_{\parallel} > 0$ and for the region where the first high-lying resonance exists), this calculation is in quite good agreement with the experiment as far as the resonances at $\vec{k}_{\parallel} = 0$ are concerned. It thus may provide the final answer to the puzzle about the origin of the so-called Swanson hump. However, before such a claim can be made one has to understand how and why self-consistency should play such an important role not only for the energy position but also for the existence of surface resonances.

VI. SUMMARY AND CONCLUSIONS

We have presented an experimental and theoretical study of the surface resonances on the (100) faces of W and Mo. We have formulated four criteria which we believe to be helpful in order to identify surface states (resonances) on solids. From our experimental study, utilizing both angle-resolved photoemission with use of synchrotron radiation and angle-integrated photoemission as well as field emission, we have documented the following properties of these resonances:

(a) There are three occupied bands of surface resonances existing in the surface Brillouin zone. They are located about 0.2, 0.6, and 3.3 (0.3, 0.8, and 4.2) eV below E_F for Mo (W). The dispersion is about 0.2 eV for the first and second bands of resonances and is about 0.3 eV for the low-lying band of resonances. All these three bands of resonances are well separated in energy.

(b) The first band of resonances is mainly d_{z^2} in character. It forms the well-known "surface-state" peak in the field-emission spectra.

(c) The second band of resonances is primarily composed of $d_{x^2-y^2}$ and $d_{zx,zy}$ orbitals. It results in a shoulder below the "surface-state" peak in both the field-emission and angle-integrated photoemission spectra. Its photoemission intensity is zero at normal exit, which implies that this second resonance is either nonexistent at $\vec{k}_{\parallel} = 0$ or possesses purely Δ_2 ($d_{x^2-y^2}$) symmetry at $\vec{k}_{\parallel} = 0$.

(d) The third band of resonances is made up of d_{z^2}, s, and p_z orbitals. It possesses Δ_1 symmetry at $\vec{k}_{\parallel} = 0$.

Except for the first band of resonances, we have been able to interpret all the other experimental facts in terms of our non-relativistic calculation of the $\vec{k}_{\parallel}$ and orbital-resolved surface density of states.[29,35]

In addition to the above ground-state properties, we have also learned from this study the following facts.

(i) The photoemission data and the field-emission data are consistent with each other.

(ii) Many-body effects are not necessary to explain the photoemission or field-emission data.

(iii) The photoemission cross sections of these surface resonances are affected microscopically by final-state band structure effects (i.e., "photo-resonances") and macroscopically by reflection and refraction effects of the photon field at the interface.

(iv) The first high-lying resonance is mainly excited by the normal component of the electric field just *outside* (i.e., due to the incoming and the reflected fields) the surface. This provides information about the spatial distribution of this resonance. The second high-lying resonance is, however, excited by the surface component of the electric field.

(v) Correct alignment and good resolution of an electron-energy analyzer are important in order to obtain meaningful experimental data.

(vi) The photoemission cross section of the first high-lying resonance exhibits "interference effects" in the plane of incidence. From these one can in principle deduce information about photoexcitation matrix elements.

VII. CONCLUDING REMARKS

For the first time, we have clearly determined the *orbital character* of these surface resonances using synchrotron radiation and, moreover, determined the correlation between the *photoexcitation* of these resonances and the *reflection* and refraction effects of the photon field at an interface. These not only resolve many historical puzzles concerning the origin of these resonances, but also provide a unique basis for the justification of a surface electronic theory. This, in turn, sheds light on the understanding of the charge distribution and the many other electronic properties pertaining to these metal surfaces. Ultimately, such microscopic level of understanding of the surface electronic structure should enable us to understand microscopically the bonding character of these metal surfaces.

*Present address: Bell Laboratories, Murray Hill, N. J. 07974.

[1] E. W. Plummer, J. W. Gadzuk, and D. R. Penn, Phys. Today 28, 63 (1975); D. E. Eastman and M. I. Nathan, ibid. 44 (1975).

[2] J. R. Schrieffer and P. Soven, Phys. Today 28, 24 (1975).

[3] J. A. Appelbaum and D. R. Hamann, Rev. Mod. Phys. 48, 479 (1976).

[4] A review covering work up to mid 1976 has been made by B. Feuerbacher and R. F. Willis, J. Phys. C 9, 169 (1976).

[5] L. W. Swanson and L. C. Crouser, Phys. Rev. Lett. 16, 389 (1966).

[6] L. W. Swanson and L. C. Crouser, Phys. Rev. Lett. 19, 1179 (1967).

[7] E. W. Plummer and J. W. Gadzuk, Phys. Rev. Lett. 25, 1493 (1970).

[8] B. J. Waclawski and E. W. Plummer, Phys. Rev. Lett. 29, 783 (1972).

[9] B. Feuerbacher and B. Fitton, Phys. Rev. Lett. 29, 786 (1972).

[10] R. D. B. Whitcutt and B. H. Blott, Phys. Rev. Lett. 23, 639 (1969).

[11] B. Feuerbacher and R. F. Willis, Phys. Rev. Lett. 37, 446 (1976).

[12] W. F. Egelhoff, J. W. Linnett, and D. L. Perry, Phys. Rev. Lett. 36, 98 (1976).

[13] C. Noguera, D. Spanjaard, D. Jepsen, Y. Ballu, C. Guillot, J. Lecante, J. Paigne, Y. Petroff, R. Pinchaux, P. Thiry, and R. Conti, Phys. Rev. Lett. 38, 1171 (1977).

[14] G. J. Lapeyre, R. J. Smith, and J. Anderson, J. Vac. Sci. Technol. 14, 384 (1977).

[15] R. F. Willis, B. Feuerbacher, and B. Fitton, Solid State Commun. 18, 1315 (1976).

[16] E. Al Khouri Nemeh, R. C. Cinti, and J. B. Hudson, J. Phys. Lett. (Paris) 35, L179 (1974).

[17] R. C. Cinti, E. Al Khoury, B. K. Chakraverty, and N. E. Christensen, Phys. Rev. B 14, 3296 (1976).

[18] D. Nagy and P. H. Cutler, Phys. Rev. 186, 651 (1969).

[19] J. W. Gadzuk, Phys. Rev. 182, 416 (1969); C. B. Duke and J. Fauchier, Surf. Sci. 32, 175 (1972).

[20] J. W. Gadzuk, J. Vac. Sci. Technol. 9, 591 (1972).

[21] R. Feder and K. Sturm, Phys. Rev. B 12, 537 (1975).

[22] J. B. Pendry and S. J. Gurman, Surf. Sci. 49, 87 (1975).

[23] F. Forstmann and J. B. Pendry, Z. Phys. 235, 35 (1970).

[24] N. Nicolaou and A. Modinos, Phys. Rev. B 11, 3687 (1975); Surf. Sci. 60, 527 (1976); A. Modinos and N. Nicolaou, Phys. Rev. B 13, 1536 (1975).

[25] M. C. Desjonqueres and F. Cyrot-Lackmann, J. Phys. F 5, 1368 (1975).

[26] N. Kar and Paul Soven, Solid State Commun. 20, 977 (1976); E. W. Plummer, Paul Soven, and N. Kar, Crit. Rev. Solid State Sci. 6, 111 (1976).

[27] N. V. Smith and L. F. Mattheiss, Phys. Rev. Lett. 37, 1494 (1976).

[28] Shang-Lin Weng, Phys. Rev. Lett. 38, 434 (1977).

[29] R. V. Kasowski, Solid State Commun. 17, 179 (1975).

[30] J. Hermanson, Solid State Commun. 22, 9 (1977).

[31] G. P. Kerker, K. M. Ho, and M. L. Cohen, Phys. Rev. Lett. 40, 1593 (1978).

[32] Additional theoretical calculations on these surface states can be found in the following papers: C. M. Bertoni, C. Calandra and F. Manghi, Solid State Commun. 23, 255 (1977); O. Bisi, C. Calandra, P. Flarioni, and F. Manghi, ibid. 21, 121 (1977); B. Laks and C. E. T. Yoncalves du Silva, ibid. 25, 401 (1978).

[33] Shang-Lin Weng and E. W. Plummer, Solid State Commun. 23, 515 (1977).

[34] Shang-Lin Weng, T. Gustafsson, and E. W. Plummer, Phys. Rev. Lett. 39, 822 (1977).

[35] Shang-Lin Weng, Ph.D. thesis (University of Pennsylvania, 1978) (unpublished).

[36] C. L. Allyn, T. Gustafsson, and E. W. Plummber, Rev. Sci. Instrum. (to be published).

[37] C. E. Kuyatt and E. W. Plummer, Rev. Sci. Instrum. 43, 108 (1972).

[38] E. M. Muller and T. T. Tsong, Field Ion Microscopy, Principles and Applications (American Elsevier, New York, 1969), p. 121.

[39] B. Feuerbacher and B. Fitton, Solid State Commun. 15, 301 (1974).

[40] J. D. Jackson, Classical Electrodynamics, 6th ed. (Wiley, New York, 1967), p. 220.

[41] J. H. Weaver, C. G. Olson, and D. W. Lynch, Phys. Rev. B 12, 1293 (1975).

[42] J. H. Weaver, D. W. Lynch, and C. G. Olson, Phys.

Rev. B 10, 501 (1974).

[43] J. B. Danese and P. Soven, Phys. Rev. B 16, 706 (1977).

[44] A. Bagchi, N. Kar, and R. G. Barrera, Phys. Rev. Lett. 40, 803 (1978).

[45] R. F. Willis, Phys. Rev. Lett. 34, 670 (1975).

[46] B. Feuerbacher and N. E. Christensen, Phys. Rev. B 10, 2373 (1974).

[47] E. W. Plummer and A. W. Bell, J. Vac. Sci. Technol. 9, 583 (1972).

[48] J. C. Slater and G. F. Koster, Phys. Rev. 94, 1498 (1954).

[49] J. Koutecky, Phys. Rev. 108, 13 (1957); J. Koutecky and M. Tomesek, Surf. Sci. 3, 333 (1965).

[50] D. Kalkstein and P. Soven, Surf. Sci. 26, 85 (1971).

[51] R. Haydock, V. Heine, M. J. Kelly, and J. B. Pendry, Phys. Rev. 869 (1972).

[52] J. W. Davenport, T. L. Einstein, and J. R. Schrieffer, Jpn. J. Appl. Phys. Suppl. 2, Part 2, 691 (1974).

[53] I. Petroff and C. R. Vieswanstan, Phys. Rev. B 4, 799 (1971).

[54] R. F. Iverson and L. Hodges, Phys. Rev. B 8, 1429 (1973).

[55] R. F. Willis, B. Feuerbacher, and N. E. Christensen, Phys. Rev. Lett. 38, 1087 (1977).

[56] L. C. Feldman, R. L. Kauffman, P. J. Silberman, R. A. Zuhr, and J. H. Barrett, Phys. Rev. Lett. 39, 38 (1977).

[57] M. K. Debe, D. A. King, and F. S. Marsh, Surf. Sci. 68, 437 (1977).

[58] M. A. van Hove and S. Y. Tong, Surf. Sci. 54, 91 (1975).

[59] B. W. Lee, A. Ignatiev, S. Y. Tong, and M. A. van Hove, J. Vac. Sci. Technol. 14, 291 (1977).